Disease Models & Mechanisms 6, 115-124 (2013) doi:10.1242/dmm.009183

Endogenous ribosomal protein L29 (RPL29): a newly identified regulator of angiogenesis in mice

Dylan T. Jones[1,2,*], Tanguy Lechertier[1], Louise E. Reynolds[1], Richard Mitter[3], Stephen D. Robinson[4], Catherine B. Kirn-Safran[5] and Kairbaan M. Hodivala-Dilke[1]

SUMMARY

Cellular ribosomal protein L29 (RPL29) is known to be important in protein synthesis, but its function during angiogenesis has never been described before. We have shown previously that mice lacking β3-integrins support enhanced tumour angiogenesis and, therefore, deletion of endothelial αvβ3 can provide a method for discovery of novel regulators of tumour angiogenesis. Here, we describe significant upregulation of RPL29 in *β3*-null endothelial cells at both the mRNA and protein level. Ex vivo, we show that VEGF-stimulated microvessel sprouting was reduced significantly in *Rpl29*-heterozygous and *Rpl29*-null aortic ring assays compared with wild-type controls. Moreover, we provide in vivo evidence that RPL29 can regulate tumour angiogenesis. Tumour blood vessel density in subcutaneously grown Lewis lung carcinomas was reduced significantly in *Rpl29*-mutant mice. Additionally, depletion of *Rpl29* using RNA interference inhibited VEGF-induced aortic ring sprouting, suggesting that anti-RPL29 strategies might have anti-angiogenic potential. Overall, our results identify that loss or depletion of RPL29 can reduce angiogenesis in vivo and ex vivo.

INTRODUCTION

Angiogenesis, the formation of new blood vessels from pre-existing vasculature, is crucial for tumour growth and cancer progression, implying that anti-angiogenic drugs are likely to be of importance in the treatment of neoplasia (Weidner et al., 1991; Bergers and Benjamin, 2003). Angiogenesis involves coordinated endothelial-cell proliferation, migration and tube formation and is influenced both by growth factors, such as vascular endothelial growth factor (VEGF), and by cell adhesion molecules such as integrins (Neufeld et al., 1999; Hodivala-Dilke et al., 2003; Olsson et al., 2006; Silva et al., 2008). A favourable shift in the local concentrations of pro-angiogenic mediators is required for tumour neovascularisation to occur (Iruela-Arispe and Dvorak, 1997; Bergers and Benjamin, 2003; Hanrahan et al., 2003; Carmeliet, 2005; Baeriswyl and Christofori, 2009; Przybylski, 2009).

The increased expression of αvβ3-integrin on newly formed vessels was considered to be a pro-angiogenic event (Sepp et al., 1994; Max et al., 1997), and αvβ3 antagonists have been shown to inhibit angiogenesis in some preclinical settings (Desgrosellier and Cheresh, 2010; Drake et al., 1995; Nicolaou et al., 1998; Storgard et al., 1999; Gutheil et al., 2000; Nabors et al., 2007). By contrast, we have shown previously that mice lacking β3-integrin exhibit enhanced tumour angiogenesis and VEGF-stimulated angiogenesis, suggesting strongly that the absence of β3-integrin confers a pro-angiogenic phenotype in endothelial cells (Reynolds et al., 2002; Reynolds et al., 2004). Indeed, *β3*-null cells have high expression of the pro-angiogenic receptor FLK1 (VEGF-receptor 2), which suggests that β3-integrin negatively regulates FLK1 expression (Reynolds et al., 2004).

To understand further the molecular basis of angiogenesis, we have exploited *β3*-null endothelial cells to identify novel genes that regulate angiogenesis. We have shown that ribosomal protein L29 (RPL29) is upregulated significantly in *β3*-null endothelial cells compared with wild-type controls. RPL29 plays an important role in protein synthesis, being a component of functionally stable ribosomes (DeLabre et al., 2002; Kirn-Safran et al., 2007). *Rpl29*-null embryonic fibroblasts have decreased rates of proliferation and protein synthesis (Kirn-Safran et al., 2007). Although a synthetic RPL29 peptide has been shown to inhibit VEGF-and FGF-induced angiogenesis via its interaction with cell surface heparin and/or heparan sulphate proteoglycans (D'Souza et al., 2008), endogenous, cellular RPL29 has not been shown to be involved in angiogenesis.

Here, we establish that RPL29 is upregulated significantly in *β3*-null endothelial cells and demonstrate that inhibition of RPL29 by genetic ablation or short interfering RNA (siRNA)-mediated depletion is sufficient to inhibit angiogenesis both in vivo and ex vivo.

RESULTS

Differential gene expression between wild-type and *β3*-null endothelial cells

We have shown previously that mice lacking β3-integrin exhibit enhanced tumour angiogenesis, suggesting strongly that the

[1]Centre for Tumour Biology, Barts Cancer Institute – a CR-UK Centre of Excellence, Queen Mary University of London, John Vane Science Centre, Charterhouse Square, London, EC1M 6BQ, UK
[2]Growth Factor group, Molecular Oncology, The Weatherall Institute of Molecular Medicine, University of Oxford, John Radcliffe Hospital, Headington, Oxford, OX3 9DS, UK
[3]Bioinformatics and Biostatistics Service, Cancer Research United Kingdom, London, WC2A 3LY, UK
[4]School of Biological Sciences, University of East Anglia, Norwich Research Park, Norwich, NR4 7TJ, UK
[5]Department of Biological Sciences, University of Delaware, Newark, DE 19716, USA
*Author for correspondence (dylan.jones@oncology.ox.ac.uk)

Received 24 November 2011; Accepted 29 June 2012

TRANSLATIONAL IMPACT

Clinical issue

Angiogenesis, the formation of new blood vessels, is required for tumour growth and progression. The potential of antiangiogenic therapy to treat cancer is illustrated by results from clinical trials in which patients were treated with Avastin (an inhibitor of angiogenesis) plus chemotherapy. However, existing treatment regimes have relatively poor efficacy, and there is much room to improve antiangiogenic cancer therapy. In addition, more work is required to elucidate the precise molecular mechanisms of angiogenic regulation in order to design rational strategies.

Results

In this paper, the authors examined gene expression in blood vessel endothelial cells isolated from mice lacking αvβ3 integrin cell adhesion protein. The authors showed previously that mice lacking β3-integrins support enhanced tumour angiogenesis, so studying mice lacking endothelial αvβ3 provides a way to discover novel regulators of tumour angiogenesis. This approach showed that cellular ribosomal protein L29 (RPL29) was markedly upregulated in *β3*-null endothelial cells at both the mRNA and protein level. Examination of aortic rings showed that VEGF-stimulated microvessel sprouting was significantly reduced in *Rpl29*-heterozygous and *Rpl29*-null mice compared with wild-type controls. Moreover, tumour blood vessel density in subcutaneously grown Lewis lung carcinomas was significantly reduced in *Rpl29*-heterozygous mice. Finally, siRNA-mediated depletion of *Rpl29* inhibited VEGF-induced aortic ring sprouting.

Implications and future directions

These findings demonstrate that loss or deletion of RPL29 in endothelial cells inhibits vascular sprouting, introducing a new regulator of angiogenesis. They also suggest that inhibition of RPL29 is a potential strategy for anti-angiogenic therapy. Notably, it has been shown that RPL29 is upregulated in some malignancies. It is conceivable that RPL29 inhibitors would target both tumour cells and the stroma (which includes endothelial cells) if used as a potential cancer therapy. Further studies will be required to discover whether targeting blood vessels with small molecules targeting RPL29 can inhibit angiogenesis.

absence of αvβ3-integrin confers a pro-angiogenic phenotype in endothelial cells (Reynolds et al., 2002). Here, we describe exploitation of *β3*-null endothelial cells to identify novel regulators of angiogenesis.

Using Illumina Bead Chips for gene expression profiling, we identified 12 genes whose expressions were increased or decreased significantly in *β3*-null endothelial cells compared with wild-type endothelial cells ($P<1\times10^{-6}$, Benferroni correction <0.05). We also identified an additional 75 genes with twofold change of expression and $P<0.01$, and 73 genes with twofold change of expression and $P<0.05$ (Fig. 1). *β3*-null mice were generated by replacing a fragment of β3-integrin gene with a neomycin resistance (NeoR) cassette (Hodivala-Dilke et al., 1999). As expected, NeoR-S was the most significantly changed gene with the highest fold change and thus acted as an excellent internal control. By contrast β3-integrin expression was decreased significantly in *β3*-null endothelial cells compared with wild-type endothelial cells. In total, 87 genes including NeoR-S and β3-integrin were expressed at significantly ($P<0.01$) higher or lower levels (at least twofold difference) in *β3*-null endothelial cells compared with wild-type controls (supplementary material Tables S1, S2).

Validation of gene expression

Real time PCR analysis of the nine most upregulated genes in *β3*-null endothelial cells showed that only Retinoic Acid Early Transcript, gamma (*Raet1γ*) and *Rpl29* mRNA expression were upregulated significantly in *β3*-null endothelial cell samples (Fig. 2A). As expected, β3-integrin mRNA levels were low in *β3*-null endothelial cells. RAET1γ is a cell surface protein that is related to major histocompatibility complex (MHC) class I protein, which binds to NKG2D found on NK cells and subsets of T-lymphocytes (Lanier, 2005). At the protein level, no change in RAET1γ expression was detectable between wild-type and *β3*-null primary endothelial cells (supplementary material Fig. S1) and was, therefore, not pursued further. By contrast, RPL29 protein levels were upregulated significantly in *β3*-null endothelial cells compared with wild-type controls (Fig. 2B,C). The *Rpl29* gene encodes a basic protein that is known to regulate protein synthesis (Liu et al., 1996; Hoke et al., 1998), is upregulated in *β3*-null endothelial cells and is, therefore, possibly important in angiogenesis. Thus, we decided to further investigate the role of RPL29 in neovascularisation processes.

RPL29 can regulate angiogenesis

We first decided to test the importance of RPL29 directly in VEGF-mediated angiogenesis. Using a genetic ablation approach, we showed that endothelial cells isolated from *Rpl29*-null mice had no detectable *Rpl29* mRNA or RPL29 protein and that *Rpl29*-heterozygous endothelial cells had approximately half-normal levels of *Rpl29* mRNA and RPL29 protein (Fig. 3A,B). VEGF-stimulated angiogenesis was then tested using ex vivo aortic ring assays. Aortic rings, isolated from wild-type, *Rpl29*-heterozygous and *Rpl29*-null embryos at embryonic day 18.5 (E18.5), were treated with VEGF or PBS and the number of emerging microvessel

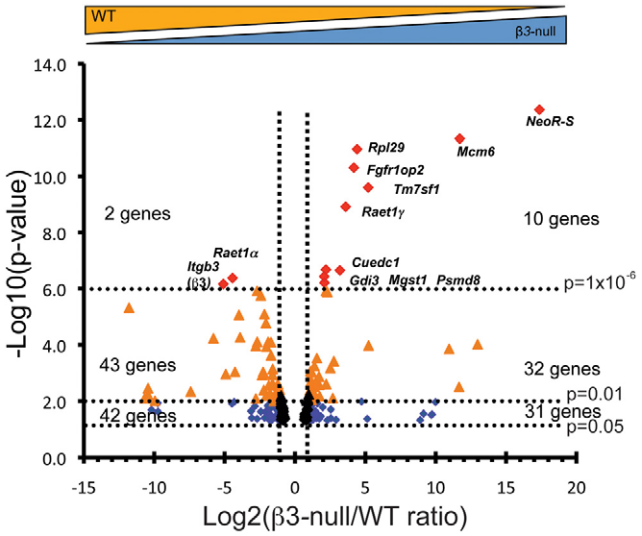

Fig. 1. Differential gene expression between *β3*-null and wild-type mouse primary endothelial cells. Volcano plot of gene expression ratios versus *P*-values. Dots represent significant differential gene expression ($P<0.05$) between *β3*-null and wild-type (WT) mouse primary endothelial cells from three independent endothelial preparations. Red diamonds, orange triangles and blue triangles represent genes with significant gene expression ranges of $P<1\times10^{-6}$ (Bonferroni correction $P<0.05$), $P=1\times10^{6}$ to 0.01 and $P=0.01$ to 0.05, respectively. The horizontal line marks the *P* -value threshold (top $P=1\times10^{-6}$, middle $P=0.01$, bottom $P=0.05$). The number of genes up- and downregulated within each significant gene expression range is given. The vertical dashed lines represent twofold differences in expression between *β3*-null and wild-type endothelial cells.

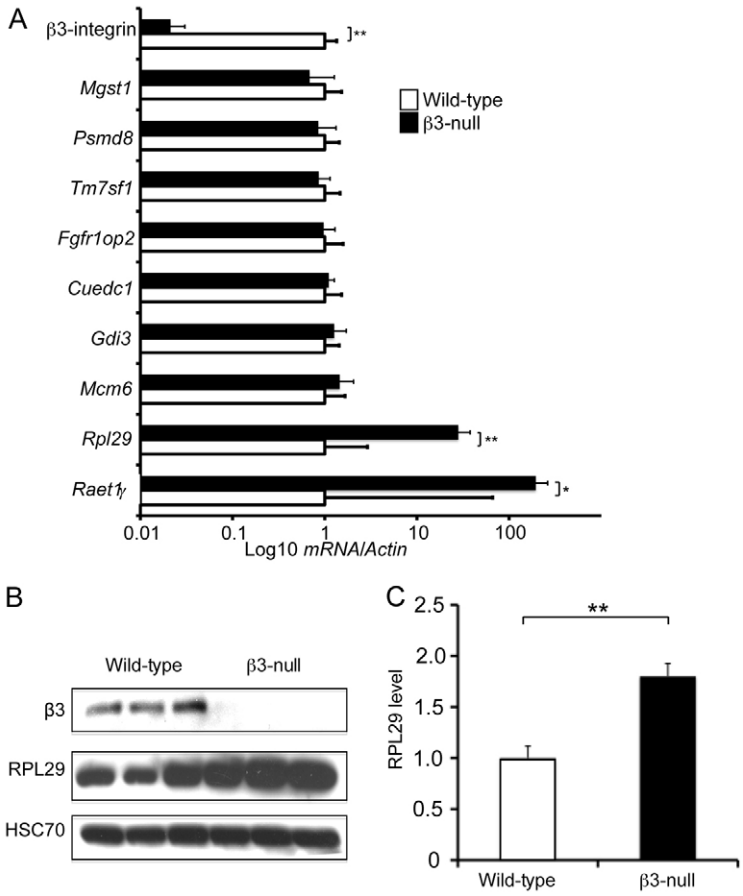

Fig. 2. Validating the differential expression of *Rpl29* mRNA and protein. (A) Real-time PCR verified that the levels of mRNA encoding β3-integrin were downregulated and that *Raet1γ* and *Rpl29* mRNA were upregulated in *β3*-null endothelial cells compared with wild-type endothelial cell controls. *β-Actin* was used as loading control, and data are represented relative to wild-type controls (*n*=3-5 samples/genotype). (B) Western blot analysis of RPL29 and β3-integrin levels in wild-type and *β3*-null endothelial cell lysates shows that RPL29 protein levels are increased in *β3*-null endothelial cells. HSC70 was used as a loading control. (C) Quantification of RPL29 protein expression in wild-type and *β3*-null endothelial cells. Western blot data are represented as densitometry readings of RPL29 protein levels relative to HSC70 (*n*=3 separate protein lysates/genotype). For all bar charts, values are given as means + s.e.m. **P*<0.05, ***P*<0.01.

sprouts counted after 5 days in three-dimensional culture. In general, VEGF-stimulation increased microvessel sprouting significantly compared with PBS-treated controls. However, VEGF-stimulated microvessel sprouting was reduced significantly in *Rpl29*-heterozygous and *Rpl29*-null aortic rings compared with wild-type controls (Fig. 3C). This change in sprouting activity did not correlate with any changes in endothelial cell proliferation (supplementary material Fig. S2). These data provide the first evidence that reduction of RPL29 levels is sufficient to inhibit VEGF-mediated angiogenesis.

Despite the reductions in VEGF-stimulated angiogenesis no changes in surface levels of VEGF-receptor 2 (FLK-1) were observed in either the *Rpl29*-heterozygous or *Rpl29*-null endothelial cells (supplementary material Fig. S3A). In addition, no changes in β3-integrin levels were observed (supplementary material Fig. S3B). Also, using siRNA against *Rpl29* in endothelial cells we did not observe a reduction in ERK phosphorylation following VEGF stimulation (supplementary material Fig. S4). These results suggest that RPL29 regulation of angiogenesis is probably not via FLK-1 or β3-integrin.

Endogenous RPL29 can regulate tumour angiogenesis

To determine whether stromal RPL29 expression affects tumour growth and angiogenesis, we injected *Rpl29*-heterozygous and wild-type mice subcutaneously with 5×10^5 luciferase-tagged Lewis lung carcinoma (LLC-luc) cells and monitored tumour growth over time. The early lethality of RPL29-null mice, in our hands, meant that it was not possible to conduct tumour growth assays in these mice. Calliper measurements of the tumours showed no significant difference in tumour sizes between the wild-type controls and *Rpl29*-heterozygous mice (Fig. 4A,B). However, the tumours grown in *Rpl29*-heterozygous mice had significantly higher levels of hypoxia (Fig. 4C). In line with this finding, bioluminescence readings, which are known to decrease in hypoxic tissues (Moriyama et al., 2008), were reduced significantly in LLC-luc tumours grown in *Rpl29*-heterozygous mice compared with wild-type controls (Fig. 4D), suggesting that reduced levels of stromal RPL29 are sufficient to increase tumour hypoxia. We did not observe any effect of *Rpl29*-heterozygozity on tumour metastasis or tumour cell proliferation and apoptosis (supplementary material Figs S5, S6).

Given that the level of tumour hypoxia can correlate with the degree of tumour vascularisation, we next analysed the blood vessel density of the tumours in *Rpl29*-heterozygous and wild-type mice. Sized-matched, 16-day-old tumours from wild-type and *Rpl29*-heterozygous mice were taken and the number of CD31-positive blood vessels per unit area across entire midline sections was assessed. Tumour blood vessel density was reduced significantly in *Rpl29*-heterozygous mice compared with wild-type controls (Fig. 5), suggesting that heterozygous levels of RPL29 are sufficient to inhibit tumour angiogenesis without affecting overall tumour burden. No significant differences in blood vessel count were observed in unchallenged skin from wild-type and *Rpl29*-heterozygous mice (supplementary material Fig. S7).

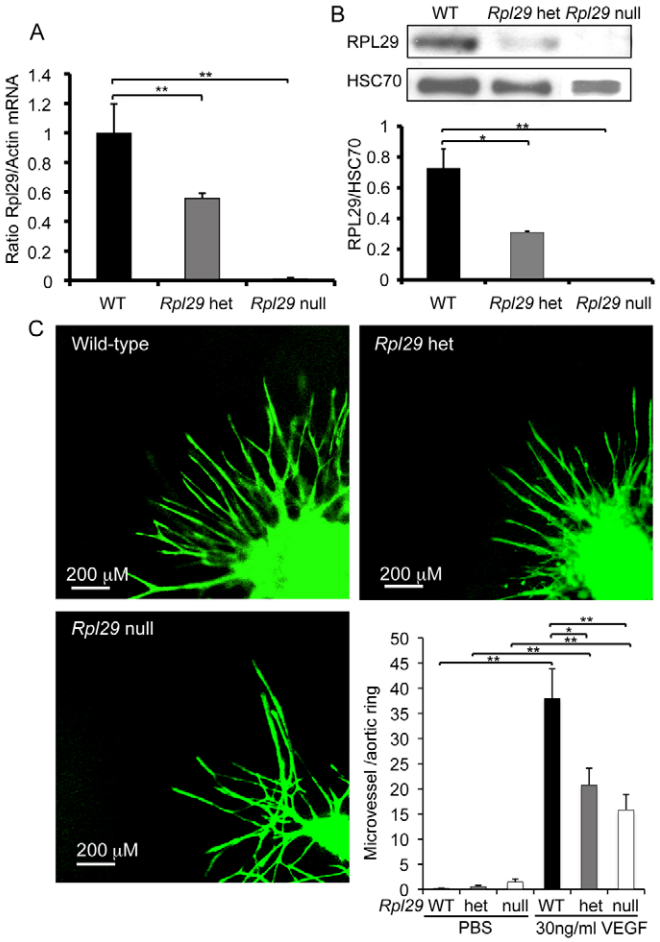

Fig. 3. Reduced VEGF-stimulated microvessel sprouting in *Rpl29*-heterozygous and *Rpl29*-deficient aortic rings. (A) RT-PCR analysis showed that *Rpl29* mRNA levels were reduced and absent in mouse endothelial cells isolated from *Rpl29*-heterozygous and *Rpl29*-null mouse lungs, respectively. *β-Actin* was used as loading control (n=3 independent samples per genotype). (B) Western blot analysis of RPL29 protein expression in wild-type, *Rpl29*-heterozygous and *Rpl29*-null mouse endothelial cells. HSC70 acts as a loading control. Bar chart represents densitometry readings from western blots of RPL29 levels relative to HSC70 (n=3 independent protein samples per genotype). (C) Wild-type, *Rpl29*-heterozygous and *Rpl29*-null aortic rings were stimulated with VEGF and microvessel sprouts counted after 5 days in culture. Representative images of microvessel sprouts immunostained for BS1-lectin are given. Bar chart represents quantification of the number of microvessels per aortic ring in the presence or absence of VEGF for all three genotypes (n=27-56 aortic rings per genotype). For all bar charts, values are given as means + s.e.m. *P<0.05, **P<0.01.

Depletion of *Rpl29* inhibits angiogenesis

We then took an RNA interference approach to test the effect of RPL29 depletion on angiogenesis in vitro. Real time PCR showed that transfection of endothelial cells with *Rpl29*-siRNA was sufficient to deplete *Rpl29* levels significantly (Fig. 6A). Although cell surface RPL29 was not detectable in cultured endothelial cells (Fig. 6B,C) it was apparent in the cell cytoplasm. siRNA-mediated depletion of RPL29 reduced cytoplasmic RPL29 protein levels significantly (Fig. 6C,D). Together, these data indicate that siRNA-mediated depletion provides a good method for the reduction of RPL29 expression. We then tested the effect of RPL29 depletion on VEGF-induced microvessel sprouting of aortic rings. Microvessel sprouting was increased in control (mock transfection) and scrambled-siRNA-transfected wild-type aortic rings after stimulation with VEGF. By contrast, *Rpl29*-depletion significantly reduced VEGF-stimulated microvessel sprouting to levels comparable with those using siRNA against Flk1 (Fig. 6E). Similar results were obtained for RPL29 depletion in *β3*-null aortic rings (supplementary material Fig. S8A). Expression of *Rpl29* mRNA was significantly reduced in aortic rings following *Rpl29*-siRNA treatment in comparison with scrambled siRNA (supplementary material Fig. S8B). This reduction in sprouting following *Rpl29*-siRNA treatment did not correlate with any changes in endothelial cell proliferation, cell migration or protein synthesis (supplementary material Figs S9-S11). These data provide evidence that RPL29 acts as a regulator of VEGF-mediated angiogenesis and that inhibition of endogenous RPL29 expression can reduce angiogenesis.

DISCUSSION

Using *β3*-null endothelial cells, as a paradigm of enhanced angiogenesis (Reynolds et al., 2002; Reynolds et al., 2004), we sought to identify novel genes that were differentially expressed in *β3*-null cells and that therefore might play a part in angiogenesis. Our work demonstrates proof-of-principle that identifying the genes that are upregulated in *β3*-null endothelial cells can identify novel modulators of angiogenesis. *Raet1γ* and *Rpl29* mRNA were upregulated significantly in *β3*-null endothelial cells. However, only RPL29 was shown to be upregulated significantly at the protein level. RPL29 is a small, highly basic polyanion binding protein with multiple functions and whose role in angiogenesis was previously unclear. Our data establish a novel role for RPL29 in angiogenesis.

We have demonstrated that heterozygous levels of RPL29 reduce microvessel sprouting in aortic rings and blood vessel density in subcutaneous tumours, and that depletion of *Rpl29* with siRNA significantly inhibits VEGF-mediated microvessel sprouting. In addition, heterozygous levels of stromal *Rpl29* were not sufficient to affect tumour bulk but did increase tumour hypoxia. However, the reduced success of available anti-angiogenic agents might be partially due to their effect on increasing hypoxia within the tumour environment, thus elevating metastasis (Ebos et al., 2009; Paez-Ribes et al., 2009). We have shown that, in our model, metastasis is not altered in *Rpl29*-heterozygous mice.

Some reports have shown that RPL29 can be expressed at the cell surface of some human tumour cells and at the interface of human foetal-maternal surface. However, in mouse cells the surface expression of RPL29 has not been demonstrated (Kirn-Safran et al., 2007) and our data corroborate this finding. At the surface of human cells, the heparin/heparan sulphate binding property of RPL29 can regulate responses to growth factors (Rohde et al., 1996; Jacobs et al., 1997; Liu et al., 1997; Rohde et al., 1998; Lander and Selleck, 2000; D'Souza et al., 2008). Indeed, application of synthetic RPL29 peptides has been shown to interfere with heparan sulphate binding to VEGF and FGF thus inhibiting angiogenesis ex vivo (D'Souza et al., 2008). These data suggest that synthetic RPL29 peptides, when used exogenously, can inhibit angiogenesis. By contrast, we show that endogenous RPL29 might play a part in enhancing angiogenesis. As to how RPL29 can regulate angiogenesis, this requires further investigation. We have data to

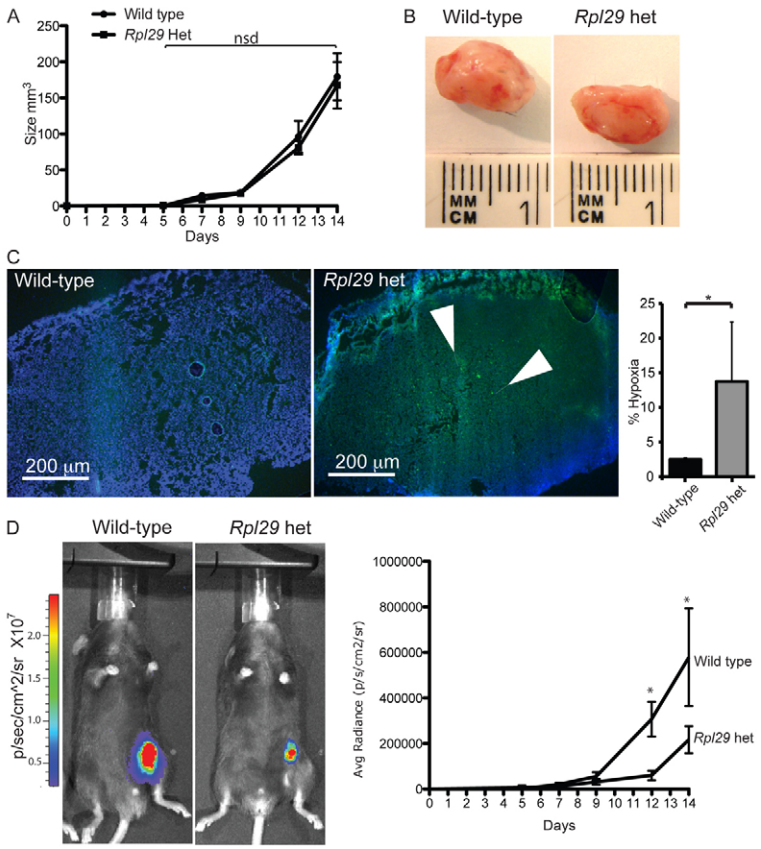

Fig. 4. Increased hypoxia in tumours grown in *Rpl29*-heterozygous mice. (A) Wild-type and *Rpl29*-heterozygous mice were injected with LLC-luc and the tumour size measured over time. No differences in tumour volumes were observed between the genotypes. (B) Images of representative tumours grown in wild-type and *Rpl29*-heterozyous mice at day 16 post-inoculation. (C) Midline sections of size-matched tumours from wild-type and *Rpl29*-heterozygous mice were analysed for hypoxia levels. Tumour-burdened wild-type and *Rpl29*-heterozygous mice were injected with pimonidazole to assess tumour hypoxia. Tumour sections were stained for pimonidazole to detect areas of tumour hypoxia (green). Hypoxia was assessed as the percentage of tumour section area occupied by pimonidazole-positive staining. Counter stain using DAPI reveal nuclei. Bar chart represents mean pimonidazole per tumour area + s.e.m. (n=4). A significant increase in hypoxia was observed in tumours grown in *Rpl29*-heterozygous mice. Arrowheads indicate pimonidazole-positive areas of tumour sections. (D) Bioluminescence images of LLC-luc tumours grown in wild-type and *Rpl29*-heterozygous mice visualised on day 14 post-inoculation. Graph represents bioluminescence readings for both genotypes over a time-course post inoculation (n=10 mice per genotype). All graphs represent means ± s.e.m. *P<0.05.

indicate that, in endothelial cells, RPL29 is not expressed at the cell surface but is expressed within the cytoplasm. Thus, its function in the regulation of protein synthesis might play a crucial role in promoting rather than inhibiting angiogenesis at the cell surface. Given that there is a growing interest in the role of endothelial metabolism in tumour angiogenesis, our work potentially provides some novel insights into this area of research.

We show that specifically targeting stromal RPL29 might not be an effective strategy for control of cancer growth, despite its anti-angiogenic potential. However, because RPL29 has been shown to play a role in maintaining cancer cells in a de-differentiated state and thus allowing uncontrolled cell proliferation to occur (Liu et al., 2006), it is conceivable that RPL29 inhibitors might have the benefit of targeting cells in the tumour and stromal compartment, including endothelial cells, if used as a potential cancer therapeutic agent (Huang et al., 2003; Liu et al., 2006). In short, our results establish RPL29 as a possible regulator of neovascularisation and provide a novel insight into the molecular control of pathological angiogenesis. We speculate that future experiments could test the efficacy of anti-RPL29 agents in combination with chemotherapeutics against cancer, and that similar anti-RPL29 strategies could possibly be applied to other vascular diseases such as arthritis and age-related macular degeneration (Kiselyov et al., 2007).

METHODS

Reagents and antibodies

VEGF-A164 was isolated in-house according to a published method (Krilleke et al., 2007). Antibodies for immunostaining, western blotting and flow cytometry were as follows: anti-CD31 (Becton Dickinson, Oxford, UK), pimonidazole hydrochloride (hypoxyprobe-1; HPI, Burlington, MA), HSC-70 (Autogen Bioclear, Oxfordshire, UK) and polyclonal anti-HIP/RPL29 peptide 43-53 antibody (kindly given to us by C.B.K.-S.) (Kirn-Safran et al., 2007). As controls, rabbit serum (Sigma, Poole, UK) or isotype-matched antibodies were used. For primary mouse endothelial cell media (MLEC) the following were used: endothelial cell growth mitogen (Abd Serotec, Oxford, UK), foetal calf serum (Biowest, Miami, FL), fibronectin (Millipore, Beeston, UK), Vitrogen (ICN Biosciences, Irvine, CA), Ham's F-12, and Dulbecco's modified Eagle's medium (DMEM; Invitrogen, Paisley, UK).

Animals

All animals were used in accord with United Kingdom Home Office regulations. $\beta 3$-integrin-deficient (Hodivala-Dilke et al., 1999) and wild-type control mice were used at 8-12 weeks of age. *Rpl29*-heterozygote mice (Kirn-Safran et al., 2007) were inter-crossed to provide wild-type, *Rpl29*-heterozygous and *Rpl29*-null mice on a C57BL6/J background. It is noteworthy that, in our hands, *Rpl29*-null mice did not survive after birth and therefore were not available for any adult tumour angiogenesis assays.

Genotyping *Rpl29*-null mice by PCR

Tail or earsnip were collected for genotyping. The primers for *Rpl29* were as follows: forward primer 5′-CATGCTAACACCAC-GCTCTT-3′; reverse primer A 5′-TGTAGTCACGGATGTC-ATCG-3′ and reverse primer B 5′-AACCTAGCTGAGAC-

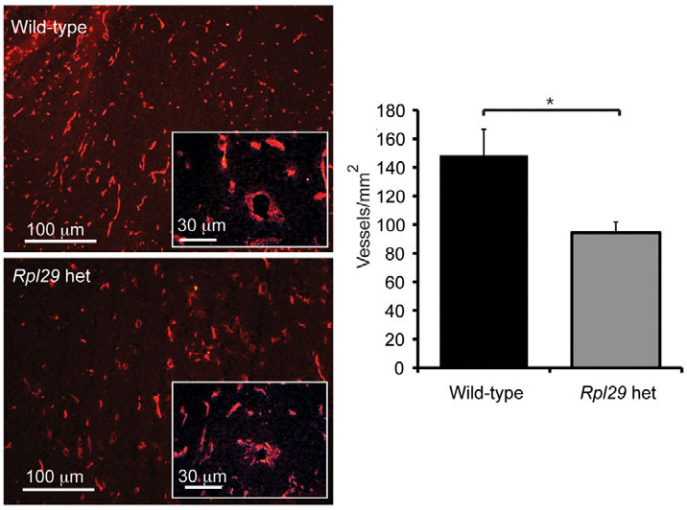

Fig. 5. Blood vessel density is decreased in LLC-luc tumours grown in wild-type and *Rpl29*-heterozygote mice. Representative images of CD31 staining in LLC-luc tumours grown in wild-type and *Rpl29*-heterozygous mice reveal the tumour blood vessels. Inserts show high magnification images. Midline sections of size-matched tumours were immunostained for CD31 and numbers of blood vessels across entire sections counted. The bar chart represents the mean + s.e.m. of the number of blood vessels per square millimetre of tumour section (*n*=4 mice per genotype), *P<0.05.

TCGCCT-3′. The reaction generates a fragment of approximately 389 base pairs for wild-type and 400 base pairs for *Rpl29* knockout mice. The amplification reactions were performed simultaneously under the same conditions as follows: 3 minutes at 94°C, 30 seconds at 94°C, 30 seconds at 60°C, 1 minute 30 seconds at 72°C for 30 cycles and a 10-minute terminal extension at 72°C.

Primary lung endothelial cell isolation

Lung endothelial cells were prepared as described previously from wild-type, *β3*-null, *Rpl29*-heterozygous and *Rpl29*-null mice (Reynolds and Hodivala-Dilke, 2006). Lungs were minced; digested with 0.1% collagenase type I (Gibco Invitrogen, Paisley, UK) in PBS for 30 minutes; passed through a 70-μm pore cell strainer (BD Falcon, Bedford, MA); resuspended in MLEC media containing a 50:50 mix of Ham's F-12:DMEM medium supplemented with 20% FCS, 20 μg/ml endothelial mitogen (Abd Serotec), 1 μg/ml heparin (Sigma), glutamine and antibiotics; and plated onto tissue-culture flasks pre-coated with a mixture of PureCol (Nutacon, The Netherlands), human plasma fibronectin (Millipore, Beeston, UK), and 0.1% gelatine. Endothelial cells were cultured and purified over a 2- to 3-week period by a series of magnetic immunosortings with Dynabeads (Invitrogen), including a single negative sort using antibodies to the Fc III/II receptor (Abd Serotec) to remove macrophages, followed by at least two positive sorts using antibodies to ICAM-2 (Abd Serotec) to enrich for the endothelial cell population.

siRNA transfection

For primary MLEC, 24 hours prior to transfection, wild-type and *β3*-null endothelial cells were counted and seeded at 6×10^4 cells per well of a six-well plate, in medium without antibiotics, to generate a 30-50% confluent monolayer on the day of transfection. For immortalised Polyoma Middle T (PmT) endothelial cells, transfection of siRNA was performed on 0.5×10^6-1×10^6 cells by electroporating them using the Basic Amaxa Nucleofector Kit designed for primary mammalian endothelial cells (Lonza, Slough, UK) following the manufacturer's instructions. For *Rpl29* and *Flk1* knockdown an ON-TARGETplus SMARTpool (Dharmacon, Thermo Fisher Scientific, Epsom, UK) was used. This pool consists of four individual siRNAs, each targeting a different region of the same mRNA. For control, a scrambled siGENOME non-targeting siRNA pool (SCM) was used (Dharmacon)

RNA extraction

Endothelial cells were purified with ICAM-2 positive selection with Dynabeads (Invitogen) to reduce possible fibroblast cell contamination. Cells were rinsed with PBS and drained thoroughly. RNA was extracted from the cells using RNeasy Mini Kit (Qiagen, Crawley, UK) following manufacturer's instructions. The quantity and the quality of RNA extracted were assessed using NanoDrop ND 1000 Spectrophotometer (NanoDrop Technologies, Wilmington, DE) and the Agilent 2100 Bio-analyzer (Agilent Technologies, Palo Alto, CA), respectively. Only RNA with RNA integrity number (RIN) of 10 was used. RNA samples were stored at −80°C.

mRNA Illumina expression analysis

A total of 250 μg of cellular RNA was amplified and labelled with Illumina TotalPrep RNA Amplification Kit (Ambion, Warrington, UK) and cRNA quantity and quality was assessed using the manufacturer's protocol. Labelled, amplified material (700 ng per array) was hybridised to the Illumina Sentrix MouseRef-6 Bead Chip according to manufacturer's instructions (Illumina, San Diego, CA). Array data processing and analysis was performed using Illumina BeadStudio and Bioconductor software (Beadarray) (Smith et al., 2010; Dunning et al., 2007). Bioconductor sample data was background-subtracted using the mean signal from the negative controls. Low signals were thresholded to 0.01. Data were quantile normalised and transformed to log base 2. Differential expression between samples was assessed using the 'limma' package (Smyth, 2005). A false discovery rate Benferroni correction below 0.05 (P<1×10^{-6}) was considered significant.

Reverse transcriptase and quantitative PCR

cDNA was synthesised by reverse transcription of RNA using the High Capacity cDNA Archive Kit (Applied Biosystems, Foster City, CA) following the manufacturer's instructions. Real-time quantitative PCR (qPCR) reactions were performed in triplicate using the Applied Biosystem StepOnePlus. Each reaction was performed in an individual well of a 96-well plate and made up to 20 μl containing 2-5 ng cDNA, 10 μl SYBR green (Applied Biosystems), 50-300 nM forward and reverse primer and H_2O. Conditions for the PCR reaction were: 2 minutes at 50°C, 10 minutes at 95°C and then 40 cycles, each consisting of 15 seconds at 95°C and 1 minute at 60°C. See supplementary material Table S3 for a list of primers and sequence (all primers were supplied by Invitrogen).

Relative quantitation of gene expression was performed using a published method (Pfaffl, 2001). In brief, comparisons were made between the number of cycles required for the fluorescence of a

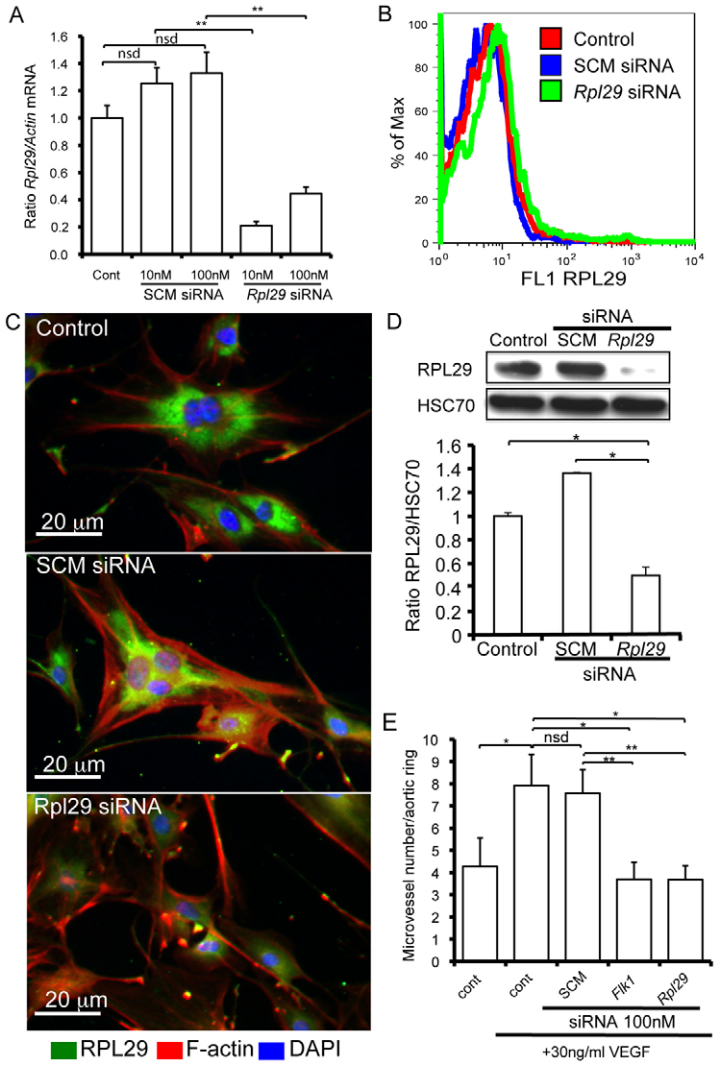

Fig. 6. siRNA-mediated depletion of *Rpl29* inhibits microvessel sprouting in wild-type mouse aortic rings. (A) RT PCR of wild-type endothelial cells transfected with either scrambled (SCM)-siRNA or *Rpl29*-siRNA at 10 nM or 100 nM concentrations. Mock-transfected cells acted as a transfection control (Cont). *β-Actin* was used as the real time PCR control for loading. Bar chart represents *Rpl29* mRNA levels relative to control and shows that this approach reduces *Rpl29* mRNA levels significantly. (n=3 samples per group). (B) Flow cytometric analysis of RPL29 surface expression in wild-type mouse endothelial cells transfected with either SCM-siRNA or *Rpl29*-siRNA, compared with mock-transfected controls (Control). RPL29 was not detectable at significant levels on the surface of mouse endothelial cells. (C) Immunofluorescence analysis reveals that RPL29 protein is detectable in the cytoplasm of mouse endothelial cells in both control and SCM-siRNA transfected samples. *Rpl29*-specific depletion, using *Rpl29*-siRNA, reduced *Rpl29* expression substantially. Phalloidin for F-Actin and DAPI were used to counterstain the cells. (D) Western blot analysis of RPL29 protein expression in wild-type mouse endothelial cell lysates after control transfection, transfection with SCM-siRNA or transfection with *Rpl29*-siRNA. HSC70 acts as a loading control. RPL29 protein levels were reduced significantly after *Rpl29*-specific depletion. Bar chart represents densitometry readings from western blots of RPL29 relative to HSC70 (n=3 independent protein samples per genotype). (E) Wild-type mouse aortic rings were either control-transfected or transfected with SCM-siRNA, Flk1-siRNA or *Rpl29*-siRNA and stimulated with 30 ng/ml VEGF. Emerging microvessels were counted at 8 days. Bar chart represents number of microvessels per aortic ring in the presence or absence of VEGF (n=12-20 aortic rings per group). *Rpl29* depletion reduced microvessel sprouting to the same extent as depletion of the major VEGF-receptor, Flk1. For all bar charts, values are given as means + s.e.m. *P<0.05, **P<0.01.

sample to reach a pre-determined threshold that lay within the exponential phase and above non-specific background. The relative ratio of gene expression was calculated as follows:

$$\text{Relative ratio} = \frac{(\text{Etarget})^{\text{DCt TARGET (mean comparator – mean sample)}}}{(\text{Eref})^{\text{DCt REF (mean comparator – mean sample)}}}, \quad (1)$$

where Etarget is the reaction efficiency of the gene of interest, Eref is the reaction efficiency of the reference gene and DCt is the cycle difference between the comparator and the sample. All calculations are based on the mean value of PCR reactions performed in triplicate.

Flow cytometric analysis of FLK1, β_3-integrin and RAET1γ

Endothelial cells were grown to 65-80% confluency, washed with PBS and trypsinised for 2-3 minutes at 37°C. After detachment, cells were washed in medium containing serum, centrifuged at 1200 rpm for 3 minutes and washed with cold sample buffer (0.1% BSA in PBS). Fluorescein isothiocyanate (FITC) and phycoerythrin (PE) were used for antibody conjugation. Single-cell suspensions were incubated with anti-FLK1-FITC antibody (Pharmingen) and anti-β_3-integrin-PE antibody (Pharmingen) in sample buffer (1:100). For expression of RAET1γ, cells were incubated with anti-RAET1γ-PE (clone CX1; BD Pharmingen) or PE rat IgG2b, κ isotype (BD Pharmingen) as isotype control in sample buffer (1:100), for 30 minutes at 4°C. After the incubation period, cells were washed three times and resuspended in a final volume of 400 µl of sample buffer. Samples were analysed for fluorescence using a Becton Dickinson FACSCalibur flow cytometer. For negative controls, IgG-matched isotype controls were used. See supplementary material Figs S1 and S3.

Caspase 3 and Ki67 staining

Frozen tumour sections were air-dried, rehydrated with PBS and fixed with ice-cold acetone for 10 minutes. Blocking buffer (1% BSA in PBS) was added to the sections for 30 minutes at room temperature then washed once with PBS. Sections were incubated with PE-PECAM (1:500; BD Pharmingen) and either Ki67 (1:100; Abcam) or Active-Caspase-3 (1:100; Cell Signaling Technology) overnight at 4°C. Sections were washed three times with PBS and incubated for 1 hour at room temperature with the relevant fluorescently conjugated secondary antibody. Sections were washed three times with PBS and mounted with Prolong Gold containing DAPI (Molecular Probes). See supplementary material Fig. S6.

Western blotting

Mouse lung endothelial cells were grown to 70-80% confluency and washed three times with ice-cold PBS and lysed in sample buffer (3% SDS, 60 mM sucrose, 65 mM Tris-Cl, pH 6.8). Lysed cells were then sonicated and spun at 13,500 ***g*** for 10 minutes at room temperature to remove insoluble material, and stored at –80ºC. For western blots, β-mercaptoethanol (1:100) and Bromophenol Blue were added to the lysates. Lysates (10-20 μg) were subjected to SDS-PAGE and transferred to nitrocellulose membranes (Hybond ECL; Amersham Biosciences, Buckinghamshire, UK). Blots were blocked in blocking buffer (5% BSA, 0.1% Tween-20 in PBS) for at least 1 hour and probed for RPL29 with 1:5000 rabbit anti-RPL29 antibody. Densitometry was performed using a gel acquisition and analysis set-up (UV Products, Cambridge, UK). Band densities were normalised to HSC-70.

Western blot analysis of ERK phosphorylation

For analysis of ERK1/2 phosphorylation following VEGF stimulation (supplementary material Fig. S4), PMT-endothelial cells were plated onto 6-cm dishes and grown in MLEC medium to 70% confluence, 2 days after transfection with *Rpl29* or scrambled siRNAs. For VEGF stimulation, cell medium was removed, cells were rinsed twice with PBS and incubated in serum-free Opti-MEM for 1 hour at 4°C. VEGF at 30 ng/ml was added to one plate and PBS in control for 30 min at 4ºC. Finally cells were incubated at 37°C for 10 minutes, rinsed once with PBS and lysed in sample buffer. Lysates (20 μg) were subjected to SDS-PAGE and transferred to nitrocellulose membranes (Hybond ECL; Amersham Biosciences) for western blotting. Blots were probed for RPL29 expression with rabbit anti-RPL29 antibody (a gift from C.B.K.-S) and ERK expression and phosphorylation with total-ERK1/2 and phosphorylated ERK1/2 antibody (Cell Signaling Technology). HSC-70 was used to determine the equality of protein loading. Densitometry was performed using a gel acquisition and analysis set-up (UV Products, Cambridge, UK). RPL29 band density was normalised to HSC-70, and the phosphorylated ERK1/2 band was normalised to total ERK.

Ex vivo aortic ring assays

Thoracic aortae were isolated from 6- to 9-week-old adult mice and prepared for culture as described previously (Nicosia and Ottinetti, 1990). However, because *Rpl29*-null mice died at birth we used E18.5 embryonic aorta from wild-type, *Rpl29*-heterozygous and *Rpl29*-null E18.5 embryonic littermates. Aortic ring assays were done either with or without siRNA transfection. For those undergoing siRNA treatment, 1-mm-thick rings were transfected in 1 ml of Opti-MEM medium with the indicated siRNA 'smart' pool duplexes (at a final concentration of 100 nM) using Oligofectamin (Invitrogen). Transfections were performed in 24-well plates with ≤24 rings per well. For real-time PCR, aortic rings were removed after 48 hours and RNA was extracted to make cDNA (supplementary material Fig. S8).

Microvessel growth on aortic rings was quantified after 5-10 days. After maximum sprouting capacity was achieved, aortic rings were fixed and stained with BS1-lectin as described (Reynolds et al., 2009), and visualised either with an epifluorescence Zeiss Axioplan microscope (Carl Zeiss, Welwyn Garden City, UK), or by confocal LSM510META microscopy (Carl Zeiss).

Mouse tumour transplantation and bioluminescence

Lewis lung carinoma cells containing firefly luciferase (0.5×10^6) were subcutaneously implanted into ten wild-type and ten *Rpl29*-heterozygote 7- to 9-week-old male C57Bl6 mice. Animal welfare was monitored daily and two-dimensional measurements of tumour growth were taken every 2-3 days with callipers during the growth period. Tumour volume was calculated using the following formula: tumour volume (mm^3) = length × width^2 × 0.52, where 0.52 is a constant used to calculate the volume of an ellipsoid. For luminescence measurement of tumour growth, mice were injected intraperitoneally with 150 μl D-Luciferin (150 μg/ml) every 2-3 days. After 10 minutes, mice were anaesthetised in a chamber containing oxygen, nitrous oxide and isoflurane. Mice were imaged using the Xenogen IVIS Lumina Imaging System (Caliper Life Science) and data collected as an average of photons per second per square centimetre per steradian ($p/s/cm^2/sr$). After 16 days, mice were injected intraperitoneally with 60 mg/kg pimonidazole hydrochloride (Hypoxyprobe) 60 minutes before the mice were killed. The tumours were collected and one half of each tumour sample was snap-frozen and the other half was fixed in 4% paraformaldehyde for histological analysis.

Histological analysis

Immunostaining of frozen mouse tumour sections to detect blood vessels with CD31 antibody was performed as described (Reynolds et al., 2002) and the samples mounted with ProLong Gold antifade reagent with DAPI (Invitrogen). For detection of the hypoxic region within tumours, sections were immunostained with hypoxyprobe-1 monoclonal antibody IgG-FITC (hypoxyprobe) against pimonidazole by following the manufacturer's instructions. Blood vessel density was presented as number of blood vessels per square millimetre, and the area of the hypoxic region measured. Midline sections were taken from age-matched, size-matched tumours and analysed using the Zeiss Axioplan microscope (Carl Zeiss).

RPL29 immunostaining of endothelial cells

Cells were grown on coverslips, washed with PBS, fixed with 4% (w/v) paraformaldehyde, and permeabilised after fixation with 0.2% (v/v) Triton X-100 containing 5% (w/v) BSA in PBS for 30 minutes. Cells on coverslips were incubated overnight in blocking buffer of PBS containing 10% (w/v) BSA and 0.15% (v/v) Tween-20. Immunostaining of RPL29 was achieved using rabbit polyclonal antisera to anti-HIP/RPL29 peptide 43-53 (Hoke et al., 1998) at 37°C for 1 hour at 1:50 dilution in blocking buffer. After appropriate washes, the secondary Alexa-Fluor-488-conjugated anti-rabbit IgG antibody (Invitrogen) was added at 37°C for 40 minutes at a 1:200 dilution in the presence of Alexa-Fluor-568-conjugated phalloidin (1:50 dilution in blocking buffer) to stain for skeletal F-Actin (Sigma). Slides were washed twice in PBS and once in water. Coverslips were mounted with ProLong Gold antifade reagent with DAPI and analysed using the Zeiss Axioplan microscope (Carl Zeiss).

FACS analysis of surface expression of RPL29

Endothelial cells were grown to 65-80% confluency, washed with PBS and trypsinised for 2-3 minutes at 37°C. After detachment, cells were washed in medium containing serum, centrifuged at

185 ***g*** for 3 minutes, and washed with cold sample buffer (0.1% BSA in PBS). Single-cell suspensions were incubated with anti-RPL29 antibody (1:100 in sample buffer) for 30 minutes at 4°C. Cells were washed three times in sample buffer and incubated with anti-rabbit Alexa Fluor 488 (Invitrogen) secondary antibody (1:100 in sample buffer) for 30 minutes at 4°C. After the incubation period, cells were washed a further three times and resuspended in a final volume of 400 µl of sample buffer. Samples were analysed for fluorescence using a Becton Dickinson FACSCalibur flow cytometer. For the negative control, rabbit serum was used.

Statistical analysis

Except where noted, data are presented as means ± s.e.m. Significance of differential gene expression between samples used in the Illumina Bead array were evaluated using false discovery rate controlled *P*-values using Benferroni correction. All other significant differences were evaluated using the Student's *t*-test; $P \leq 0.05$ was considered statistically significant.

ACKNOWLEDGEMENTS

We thank Bruce Williams for help with the in vivo experiments.

COMPETING INTERESTS

The authors declare that they do not have any competing or financial interests.

AUTHOR CONTRIBUTIONS

Conceived and designed the experiments: D.T.J. and K.M.H.-D. Performed the experiments: D.T.J., T.L., L.E.R. and S.D.R. Analyzed the data: D.T.J., T.L., L.E.R., S.D.R. and R.M. Contributed and generated mice: C.B.K.-S. Wrote the paper: D.T.J. and K.M.H.-D.

FUNDING

This work was funded by Breast Cancer Campaign [BCC 2008 MayPR07 to D.T.J. and K.M.H.-D.] and Cancer Research UK [CRUK C8212_A12007 to T.L., L.E.R. and S.D.R.]. Generation of RPL29-null/het mice was funded by National Institutes of Health [grant number P20-RR016458 to C.B.K.-S.]. Microarray data analysis by R.M. was core funded by CRUK.

SUPPLEMENTARY MATERIAL

Supplementary material for this article is available at
http://dmm.biologists.org/lookup/suppl/doi:10.1242/dmm.009183/-/DC1

REFERENCES

Baeriswyl, V. and Christofori, G. (2009). The angiogenic switch in carcinogenesis. *Semin. Cancer Biol.* **19**, 329-337.

Bergers, G. and Benjamin, L. E. (2003). Tumorigenesis and the angiogenic switch. *Nat. Rev. Cancer* **3**, 401-410.

Carmeliet, P. (2005). VEGF as a key mediator of angiogenesis in cancer. *Oncology* **69 Suppl. 3**, 4-10.

D'Souza, S., Yang, W., Marchetti, D., Muir, C., Farach-Carson, M. C. and Carson, D. D. (2008). HIP/RPL29 antagonizes VEGF and FGF2 stimulated angiogenesis by interfering with HS-dependent responses. *J. Cell Biochem.* **105**, 1183-1193.

DeLabre, M. L., Kessl, J., Karamanou, S. and Trumpower, B. L. (2002). RPL29 codes for a non-essential protein of the 60S ribosomal subunit in Saccharomyces cerevisiae and exhibits synthetic lethality with mutations in genes for proteins required for subunit coupling. *Biochim. Biophys. Acta* **1574**, 255-261.

Desgrosellier, J. S. and Cheresh, D. A. (2010). Integrins in cancer: biological implications and therapeutic opportunities. *Nat. Rev. Cancer* **10**, 9-22.

Drake, C. J., Cheresh, D. A. and Little, C. D. (1995). An antagonist of integrin alpha v beta 3 prevents maturation of blood vessels during embryonic neovascularization. *J. Cell Sci.* **108**, 2655-2661.

Dunning, M. J., Smith, M. L., Ritchie, M. E. and Tavare, S. (2007). Beadarray: R classes and methods for Illumina bead-based data. *Bioinformatics* **23**, 2183-2184.

Ebos, J. M., Lee, C. R., Cruz-Munoz, W., Bjarnason, G. A., Christensen, J. G. and Kerbel, R. S. (2009). Accelerated metastasis after short-term treatment with a potent inhibitor of tumor angiogenesis. *Cancer Cell* **15**, 232-239.

Gutheil, J. C., Campbell, T. N., Pierce, P. R., Watkins, J. D., Huse, W. D., Bodkin, D. J. and Cheresh, D. A. (2000). Targeted antiangiogenic therapy for cancer using Vitaxin: a humanized monoclonal antibody to the integrin alphavbeta3. *Clin. Cancer Res.* **6**, 3056-3061.

Hanrahan, V., Currie, M. J., Gunningham, S. P., Morrin, H. R., Scott, P. A., Robinson, B. A. and Fox, S. B. (2003). The angiogenic switch for vascular endothelial growth factor (VEGF)-A, VEGF-B, VEGF-C, and VEGF-D in the adenoma-carcinoma sequence during colorectal cancer progression. *J. Pathol.* **200**, 183-194.

Hodivala-Dilke, K. M., McHugh, K. P., Tsakiris, D. A., Rayburn, H., Crowley, D., Ullman-Cullere, M., Ross, F. P., Coller, B. S., Teitelbaum, S. and Hynes, R. O. (1999). Beta3-integrin-deficient mice are a model for Glanzmann thrombasthenia showing placental defects and reduced survival. *J. Clin. Invest.* **103**, 229-238.

Hodivala-Dilke, K. M., Reynolds, A. R. and Reynolds, L. E. (2003). Integrins in angiogenesis: multitalented molecules in a balancing act. *Cell Tissue Res.* **314**, 131-144.

Hoke, D. E., Regisford, E. G., Julian, J., Amin, A., Begue-Kirn, C. and Carson, D. D. (1998). Murine HIP/L29 is a heparin-binding protein with a restricted pattern of expression in adult tissues. *J. Biol. Chem.* **273**, 25148-25157.

Huang, D., Chen, W., He, R., Yu, F., Zhang, Z. and Qiu, W. (2003). Different cDNA microarray patterns of gene expression reflecting changes during metastatic progression in adenoid cystic carcinoma. *World J. Surg. Oncol.* **1**, 28.

Iruela-Arispe, M. L. and Dvorak, H. F. (1997). Angiogenesis: a dynamic balance of stimulators and inhibitors. *Thromb. Haemost.* **78**, 672-677.

Jacobs, A. L., Julian, J., Sahin, A. A. and Carson, D. D. (1997). Heparin/heparan sulfate interacting protein expression and functions in human breast cancer cells and normal breast epithelia. *Cancer Res.* **57**, 5148-5154.

Kirn-Safran, C. B., Oristian, D. S., Focht, R. J., Parker, S. G., Vivian, J. L. and Carson, D. D. (2007). Global growth deficiencies in mice lacking the ribosomal protein HIP/RPL29. *Dev. Dyn.* **236**, 447-460.

Kiselyov, A., Balakin, K. V. and Tkachenko, S. E. (2007). VEGF/VEGFR signalling as a target for inhibiting angiogenesis. *Expert Opin. Investig. Drugs* **16**, 83-107.

Krilleke, D., DeErkenez, A., Schubert, W., Giri, I., Robinson, G. S., Ng, Y. S. and Shima, D. T. (2007). Molecular mapping and functional characterization of the VEGF164 heparin-binding domain. *J. Biol. Chem.* **282**, 28045-28056.

Lander, A. D. and Selleck, S. B. (2000). The elusive functions of proteoglycans: in vivo veritas. *J. Cell Biol.* **148**, 227-232.

Lanier, L. L. (2005). NK cell recognition. *Annu. Rev. Immunol.* **23**, 225.

Liu, J. J., Huang, B. H., Zhang, J., Carson, D. D. and Hooi, S. C. (2006). Repression of HIP/RPL29 expression induces differentiation in colon cancer cells. *J. Cell Physiol.* **207**, 287-292.

Liu, S., Smith, S. E., Julian, J., Rohde, L. H., Karin, N. J. and Carson, D. D. (1996). cDNA cloning and expression of HIP, a novel cell surface heparan sulfate/heparin-binding protein of human uterine epithelial cells and cell lines. *J. Biol. Chem.* **271**, 11817-11823.

Liu, S., Hoke, D., Julian, J. and Carson, D. D. (1997). Heparin/heparan sulfate (HP/HS) interacting protein (HIP) supports cell attachment and selective, high affinity binding of HP/HS. *J. Biol. Chem.* **272**, 25856-25862.

Max, R., Gerritsen, R. R., Nooijen, P. T., Goodman, S. L., Sutter, A., Keilholz, U., Ruiter, D. J. and De Waal, R. M. (1997). Immunohistochemical analysis of integrin alpha vbeta3 expression on tumor-associated vessels of human carcinomas. *Int. J. Cancer* **71**, 320-324.

Moriyama, E. H., Niedre, M. J., Jarvi, M. T., Mocanu, J. D., Moriyama, Y., Subarsky, P., Li, B., Lilge, L. D. and Wilson, B. C. (2008). The influence of hypoxia on bioluminescence in luciferase-transfected gliosarcoma tumor cells in vitro. *Photochem. Photobiol. Sci.* **7**, 675-680.

Nabors, L. B., Mikkelsen, T., Rosenfeld, S. S., Hochberg, F., Akella, N. S., Fisher, J. D., Cloud, G. A., Zhang, Y., Carson, K., Wittemer, S. M. et al. (2007). Phase I and correlative biology study of cilengitide in patients with recurrent malignant glioma. *J. Clin. Oncol.* **25**, 1651-1657.

Neufeld, G., Cohen, T., Gengrinovitch, S. and Poltorak, Z. (1999). Vascular endothelial growth factor (VEGF) and its receptors. *FASEB J.* **13**, 9-22.

Nicolaou, K. C., Trujillo, J. I., Jandeleit, B., Chibale, K., Rosenfeld, M., Diefenbach, B., Cheresh, D. A. and Goodman, S. L. (1998). Design, synthesis and biological evaluation of nonpeptide integrin antagonists. *Bioorg. Med. Chem.* **6**, 1185-1208.

Nicosia, R. F. and Ottinetti, A. (1990). Modulation of microvascular growth and morphogenesis by reconstituted basement membrane gel in three-dimensional cultures of rat aorta: a comparative study of angiogenesis in matrigel, collagen, fibrin, and plasma clot. *In Vitro Cell Dev. Biol.* **26**, 119-128.

Olsson, A. K., Dimberg, A., Kreuger, J. and Claesson-Welsh, L. (2006). VEGF receptor signalling-in control of vascular function. *Nat. Rev. Mol. Cell Biol.* **7**, 359-371.

Paez-Ribes, M., Allen, E., Hudock, J., Takeda, T., Okuyama, H., Vinals, F., Inoue, M., Bergers, G., Hanahan, D. and Casanovas, O. (2009). Antiangiogenic therapy elicits malignant progression of tumors to increased local invasion and distant metastasis. *Cancer Cell* **15**, 220-231.

Pfaffl, M. W. (2001). A new mathematical model for relative quantification in real-time RT-PCR. *Nucleic Acids Res.* **29**, e45.

Przybylski, M. (2009). A review of the current research on the role of bFGF and VEGF in angiogenesis. *J. Wound Care* **18**, 516-519.

Reynolds, A. R., Reynolds, L. E., Nagel, T. E., Lively, J. C., Robinson, S. D., Hicklin, D. J., Bodary, S. C. and Hodivala-Dilke, K. M. (2004). Elevated Flk1 (vascular endothelial growth factor receptor 2) signaling mediates enhanced angiogenesis in beta3-integrin-deficient mice. *Cancer Res.* **64**, 8643-8650.

Reynolds, A. R., Hart, I. R., Watson, A. R., Welti, J. C., Silva, R. G., Robinson, S. D., Da Violante, G., Gourlaouen, M., Salih, M., Jones, M. C. et al. (2009). Stimulation of tumor growth and angiogenesis by low concentrations of RGD-mimetic integrin inhibitors. *Nat. Med.* **15**, 392-400.

Reynolds, L. E. and Hodivala-Dilke, K. M. (2006). Primary mouse endothelial cell culture for assays of angiogenesis. *Methods Mol. Med.* **120**, 503-509.

Reynolds, L. E., Wyder, L., Lively, J. C., Taverna, D., Robinson, S. D., Huang, X., Sheppard, D., Hynes, R. O. and Hodivala-Dilke, K. M. (2002). Enhanced pathological angiogenesis in mice lacking beta3 integrin or beta3 and beta5 integrins. *Nat. Med.* **8**, 27-34.

Rohde, L. H., Julian, J., Babaknia, A. and Carson, D. D. (1996). Cell surface expression of HIP, a novel heparin/heparan sulfate binding protein, of human uterine epithelial cells and cell lines. *J. Biol. Chem.* **271**, 11824-11830.

Rohde, L. H., Janatpore, M. J., McMaster, M. T., Fisher, S., Zhou, Y., Lim, K. H., French, M., Hoke, D., Julian, J. and Carson, D. D. (1998). Complementary expression of HIP, a cell-surface heparan sulfate binding protein, and perlecan at the human fetal-maternal interface. *Biol. Reprod.* **58**, 1075-1083.

Sepp, N. T., Li, L. J., Lee, K. H., Brown, E. J., Caughman, S. W., Lawley, T. J. and Swerlick, R. A. (1994). Basic fibroblast growth factor increases expression of the alpha v beta 3 integrin complex on human microvascular endothelial cells. *J. Invest. Dermatol.* **103**, 295-299.

Silva, R., D'Amico, G., Hodivala-Dilke, K. M. and Reynolds, L. E. (2008). Integrins: the keys to unlocking angiogenesis. *Arterioscler. Thromb. Vasc. Biol.* **28**, 1703-1713.

Smith, M. L., Dunning, M. J., Tavare, S. and Lynch, A. G. (2010). Identification and correction of previously unreported spatial phenomena using raw Illumina BeadArray data. *BMC Bioinformatics* **11**, 208.

Smyth, G. K. (2005). Limma: linear models for microarray data. In *Bioinformatics and Computational Biology Solutions using R and Bioconductor* (ed. R. Gentleman, V. Carey, S. Dudoit, R. Irizarry and W. Huber), pp. 397-420. New York: Springer.

Storgard, C. M., Stupack, D. G., Jonczyk, A., Goodman, S. L., Fox, R. I. and Cheresh, D. A. (1999). Decreased angiogenesis and arthritic disease in rabbits treated with an alphavbeta3 antagonist. *J. Clin. Invest.* **103**, 47-54.

Weidner, N., Semple, J. P., Welch, W. R. and Folkman, J. (1991). Tumor angiogenesis and metastasis-correlation in invasive breast carcinoma. *N. Engl. J. Med.* **324**, 1-8.

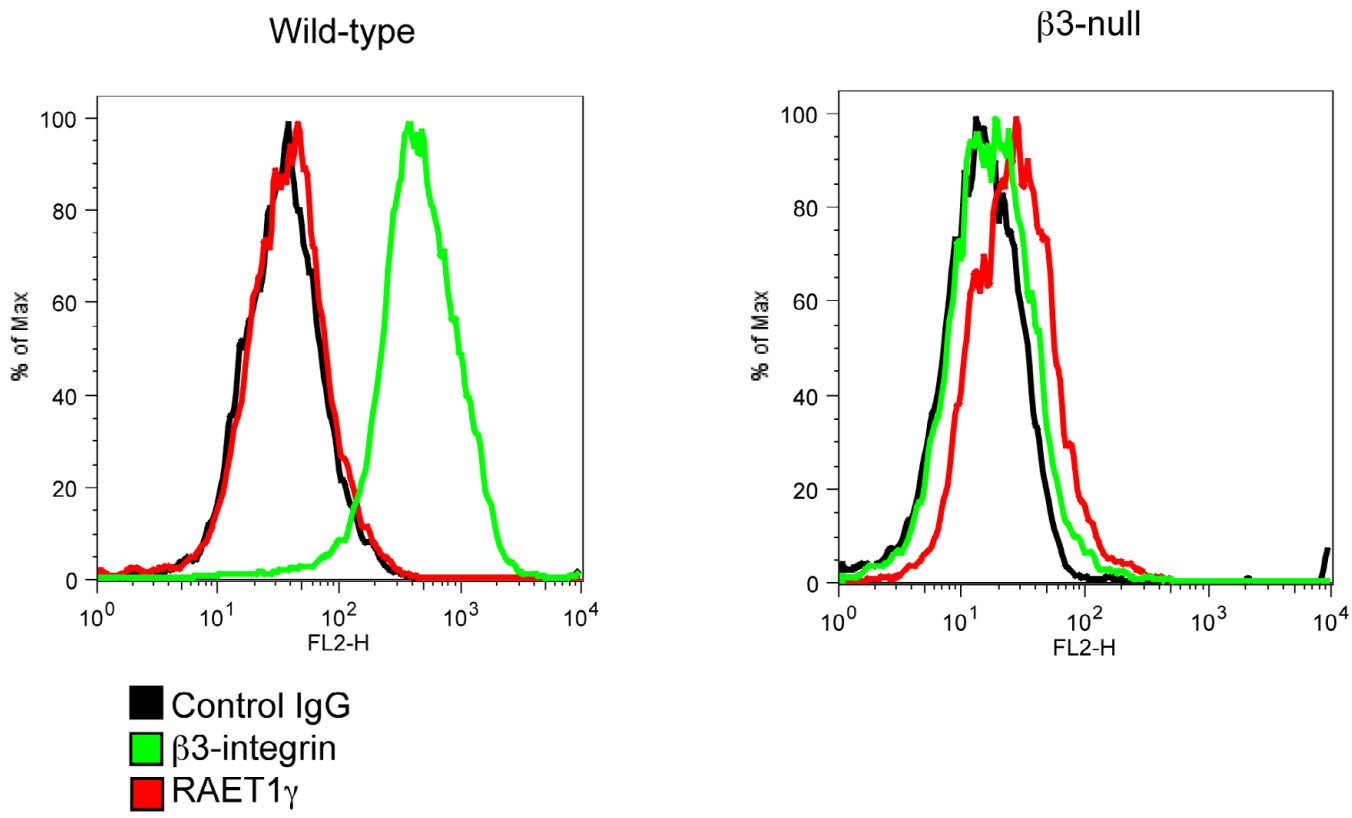

Fig. S1. Flow cytometric analysis of RAET1γ surface expression in wild-type and β3-null endothelial cells. RAET1γ was not detectable on the surface of mouse endothelial cells. Mouse IgG1 was used as negative control, and antibody against β3-integrin was used to confirm β3-integrin deficiency in β*3*-null endothelial cells.

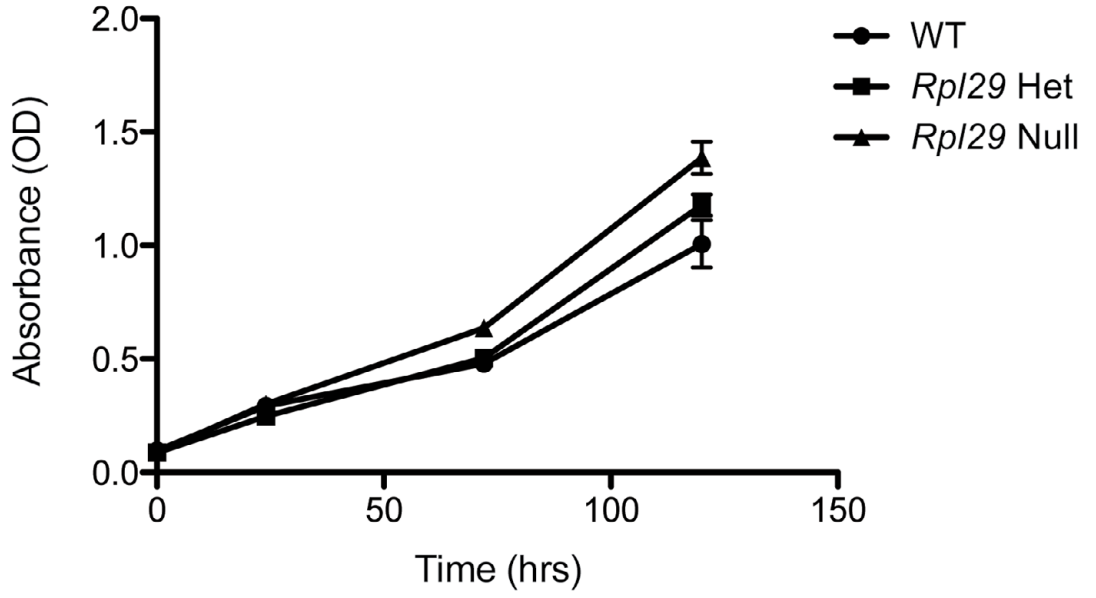

Fig. S2. Cell proliferation assay of wild-type, Rpl29-heterozygous and Rpl29-null endothelial cells. Two thousand cells were seeded into each well of a 96-well plate (Coultar) pre-coated with a mixture of PureCol (Nutacon, Netherlands), human plasma fibronectin (Millipore) and 0.1% gelatine. Cell viability was measured using cell proliferation reagent WST1 (Roche) following manufacturer's protocol at different time points. No reduction in viability was observed in *Rpl29*-heterozygous and *Rpl29*-null endothelial cells in comparison to wild-type endothelial cells (n=3, mean ± s.e.m.).

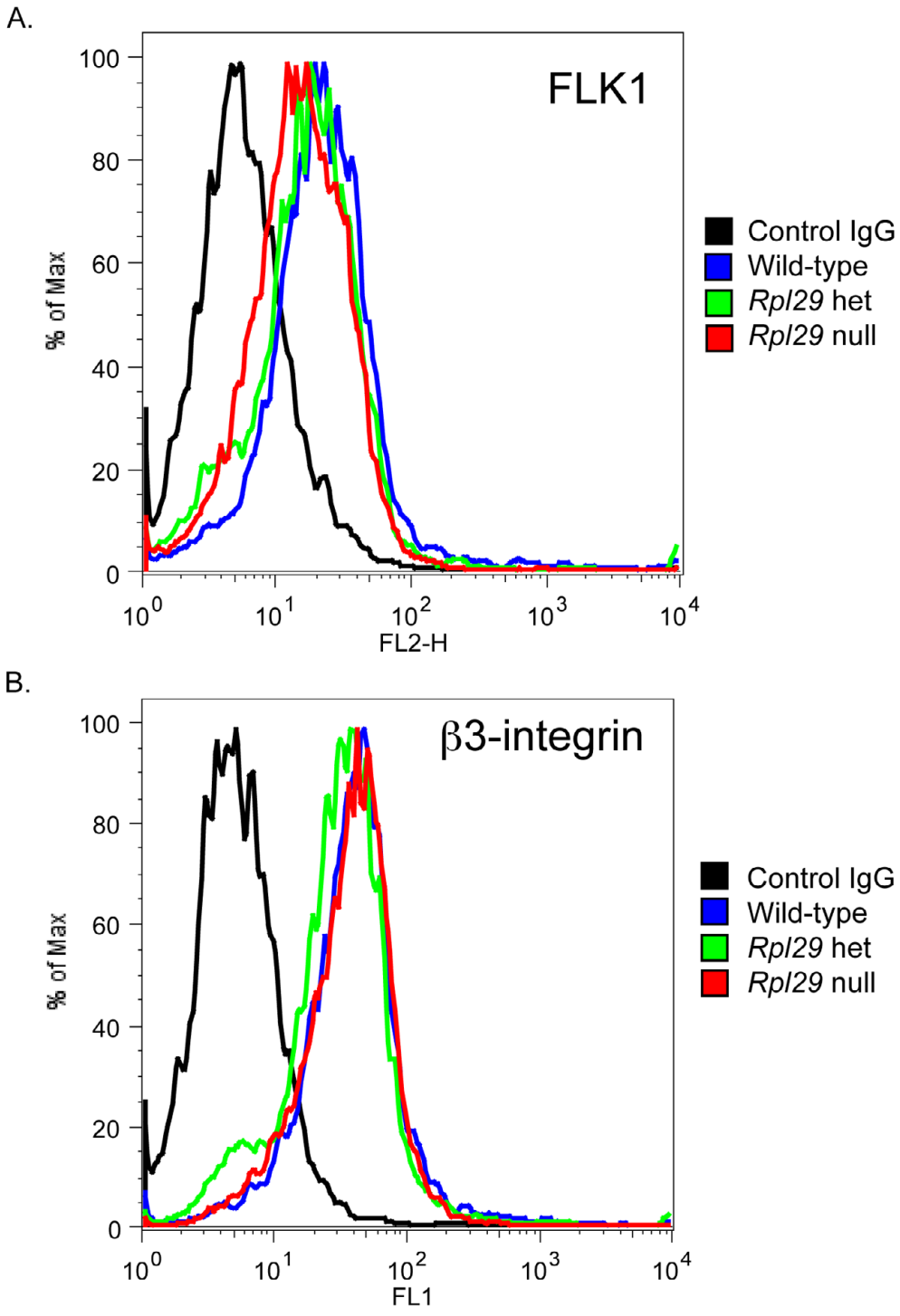

Fig. S3. Flow cytometric analysis of FLK1 and β3-integrin in Rpl29-wild-type, Rpl29-heterozygous and Rpl29-null primary endothelial cells. Mouse IgG1 was used as negative control. No changes in surface expression of either (A) FLK1 or (B) β3 integrin were observed in *Rpl29*-heterozygous or *Rpl29*-null endothelial cells when compared with wild-type controls.

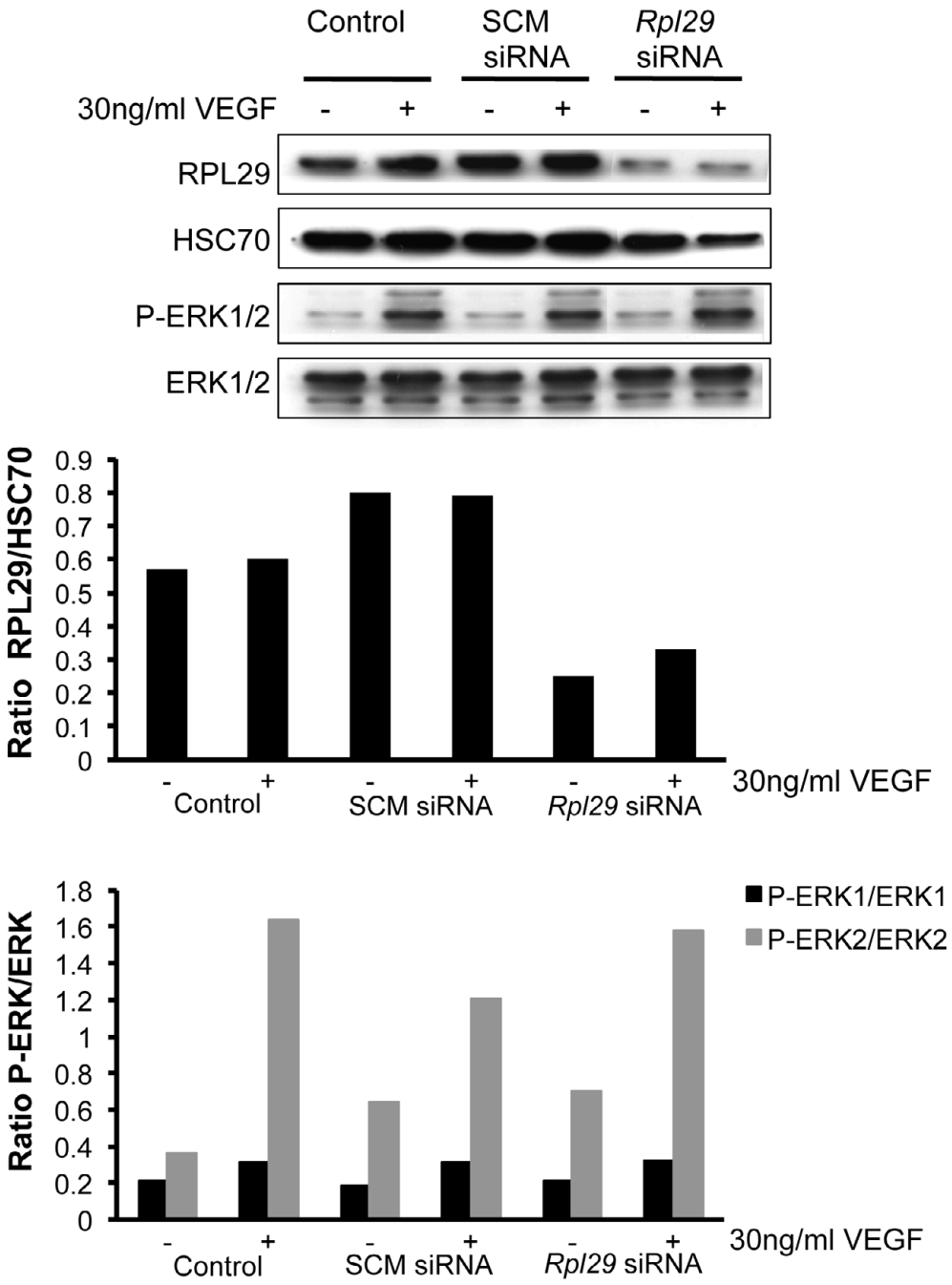

Fig. S4. VEGF-stimulated ERK-phosphorylation. Western blot analysis of pERK1/2 levels to total ERK1/2 in endothelial cells treated with SCM and *Rpl29*-siRNA show that pERK1/2 protein levels were not decreased following *Rpl29* knockdown with siRNA in comparison to SCM-siRNA when cells were exposed to VEGF. Bar charts represent densitometry readings of RPL29 levels were compared to loading control HSC70 and pERK1/2 protein levels relative to total ERK1/2.

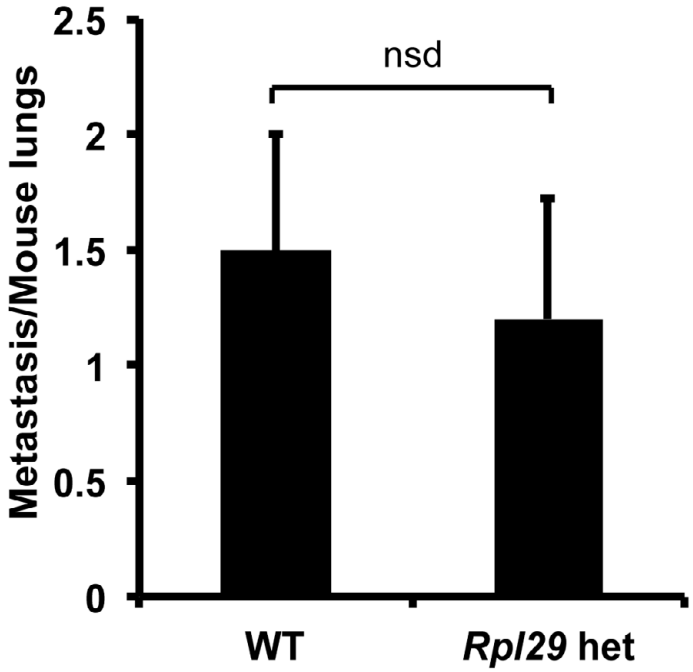

Fig. S5. Metastatic analysis of LLC grown in wild-type and Rpl29-heterozygous mice. Lewis Lung Carcinoma tumour cells (0.5 x 10^6 cells) were injected subcutaneously into the flank of 8-week-old WT and *Rpl29*-heterozygous mice and tumours were allowed to grow for 14 days. Size-matched tumours were ressected and tumours allowed to metastasise to the lungs. The mice were then killed 6 weeks later at which point they showed no adverse effects. Lungs were removed from the mice and examined for surface metastases. No significant difference in lung metastasis was observed between wild-type and Rpl29-null mice. Metastasis was measured by counting LLC metastasis on the surface of lungs/mouse (*n*=4-5, mean ± s.e.m.).

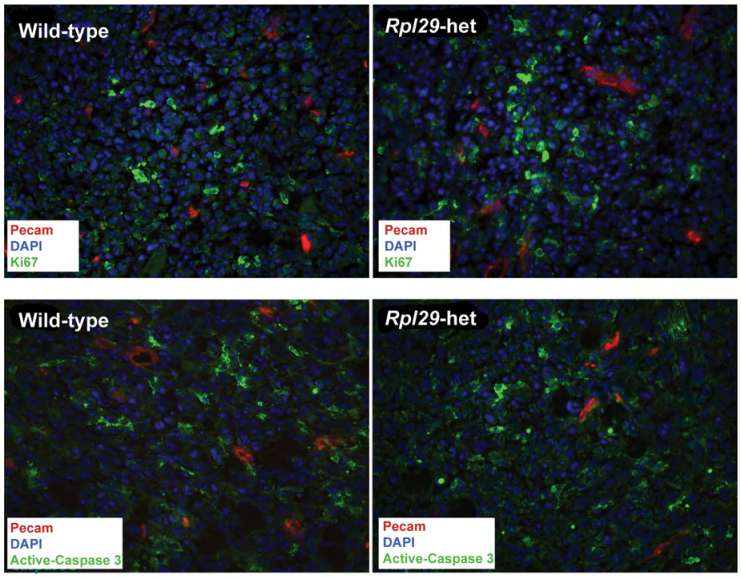

Fig. S6. Tumour proliferation and apoptosis analysis. No gross difference was observed in cell proliferation and apoptosis in LLC tumours from wild-type and *Rpl29*-heterozygous mice. Representative images of Ki67, Active-Caspase-3 and PECAM staining in size matched age matched LLC tumours grown in wild-type and *Rpl29*-heterozygous mice. Sections were counter stained with DAPI to reveal nuclei.

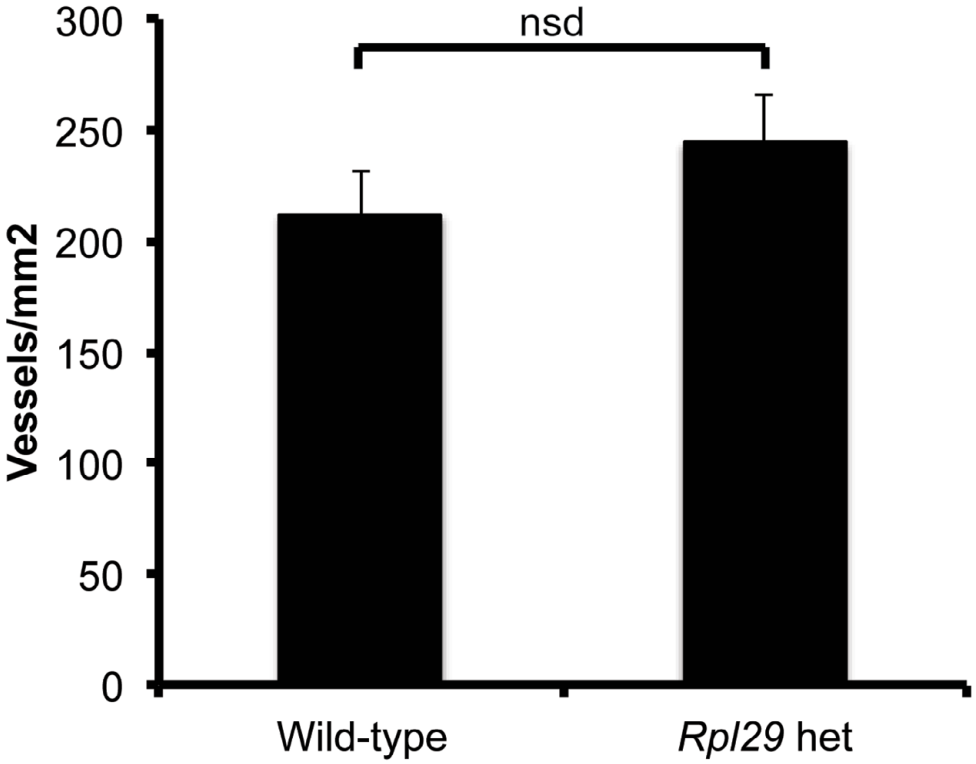

Fig. S7. Blood vessels density in the skin from wild-type and Rpl29-heterozygous mice. No significant difference was observed in blood vessel density in the skin between wild-type and *Rpl29*-heterozygous mice. Bar chart represents mean number blood vessels/mm^2 of dermal section (mean ± s.e.m.; n=7 mice per genotype; nsd, not significant).

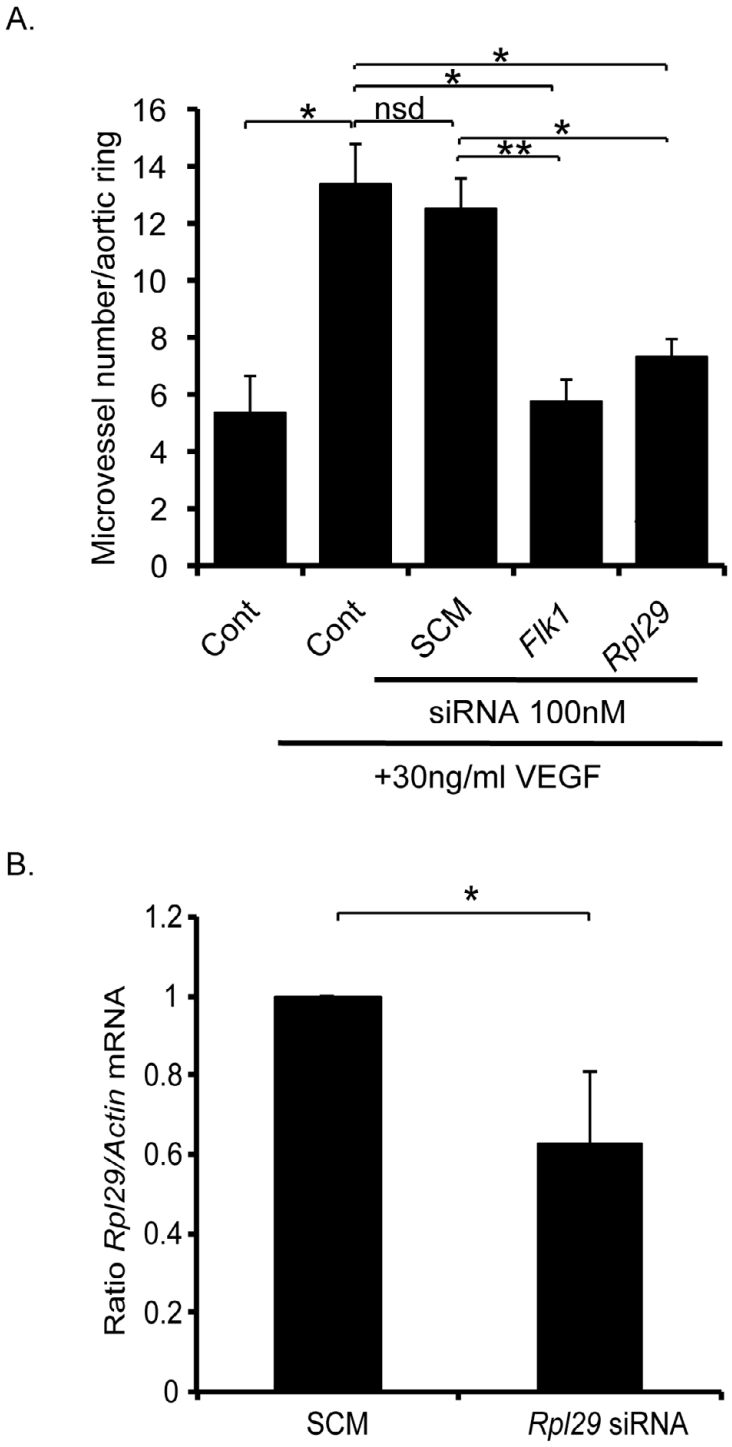

Fig. S8. Aortic ring assay following Rpl29-siRNA treatment. Depletion of Rpl29 with siRNA inhibits microvessel sprouting in β3-null aortic rings. (A) Quantitation of VEGF stimulated microvessel sprouting following treatment with SCM, *Rpl29* or *Flk1* siRNA in β*3*-null aortic rings on day 8. VEGF stimulated the number of microvessel sprouts emerging for aortic rings in Cont and SCM-siRNA treated samples. *Rpl29*-depletion reduced VEGF-stimulated microvessel sprouting to level similar to *Flk1*-depletion (mean ± s.e.m., **P*<0.05, ***P*<0.01, *n*=12-20 aortic rings per treatment). (B) Real-time PCR to validate knockdown of *Rpl29* in aortic rings following treatment with either 100nM SCM or *Rpl29* siRNA (mean ± s.e.m.,***P* <0.01, *n*=3 per group).

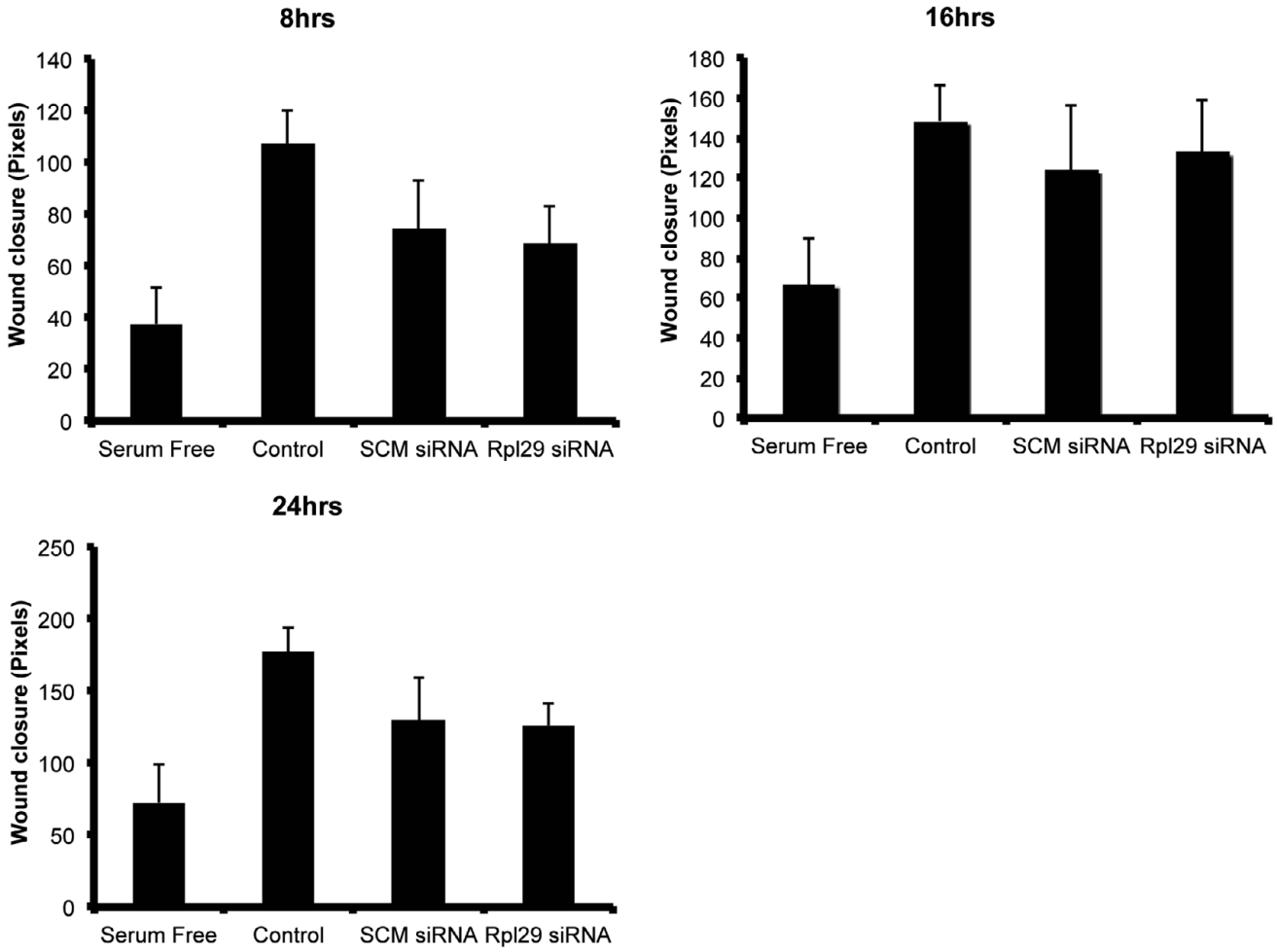

Fig. S9. Cell proliferation assay of PMT-endothelial cells treated with Rpl29 siRNA. No significant difference was observed in endothelial cell proliferation following *Rpl29* siRNA treatment in comparison to SCM siRNA and control sample using WST-1 assay (n=3, mean ± s.e.m.).

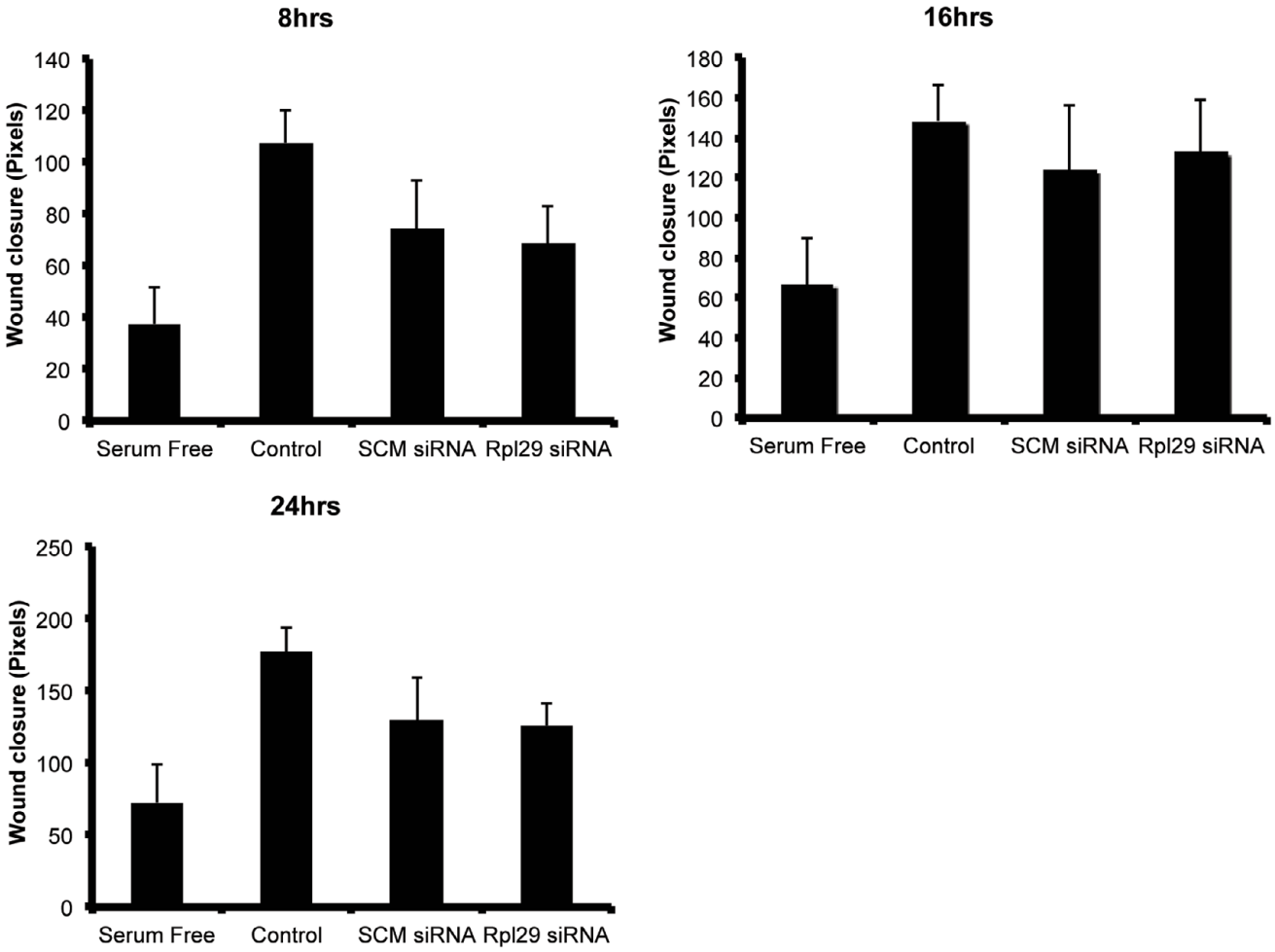

Fig. S10. Cell migration assay. Six-well plates were coated with a mixture of PureCol (Nutacon), human plasma fibronectin (Millipore), and 0.1% gelatine and seeded with 300,000 endotheilal cells per well. Cells were allowed to proliferate until confluent, washed with Opti-MEM and incubated for 2 hours in Opti-MEM 2.5% FCS. Cells in each well were scratched in a straight line with a P200 tip, and media was exchanged with a fresh Opti-MEM 2.5% FCS media with or without 30 ng/ml VEGFA. An inverted time-lapse microscope was used to follow wound healing due to cell migration for up to 24 hours, and data was analysed using ImageJ. No significant difference was observed in serum-stimulated endothelial cell migration between 8 and 24 hours between samples treated with *Rpl29* and SCM siRNA. Values are given as representations of wound closure in pixels.

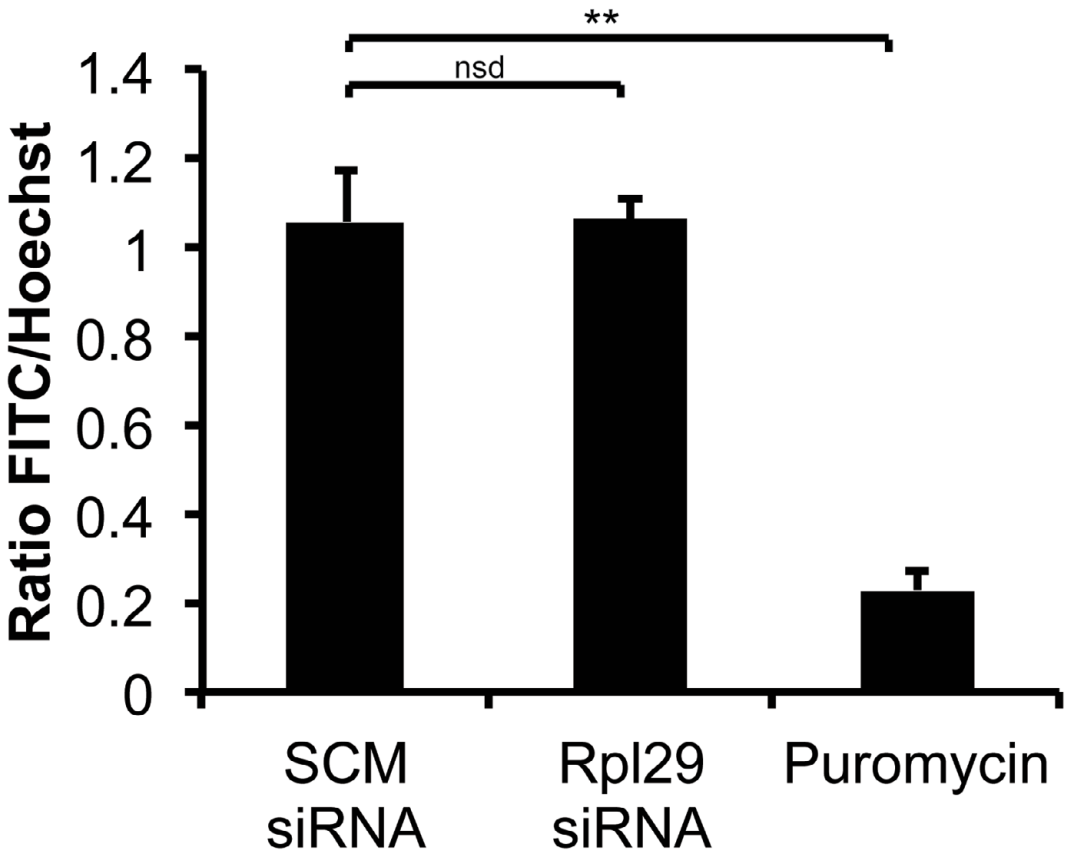

Fig. S11. Protein synthesis assay. Ten thousand cells were plated in each well of a 96-well plate pre-coated with PureCol (Nutacon), human plasma fibronectin (Millipore) and 0.1% gelatine. Protein synthesis was measured using Click-iT AHA Alexa Fluor 488 Protein Synthesis HCS Assay (Invitrogen) following the manufacturers protocol with methionine-free RPMI (Invitrogen). No significant difference was observed in protein synthesis between samples treated with *Rpl29* and SCM siRNA. Puromycin (1μM) was used as a positive control for protein synthesis inhibition. (n=3; nsd, not significant; **P<0.01).

Table S1. List of genes whose expression was upregulated in β*3*-null endothelial cells compared with wild-type (*P*<0.01).

Symbol	Accession	*P*-value	Definition
NeoR		4.4E-13	Neomycin resistant gene
Mcm6	NM_008567.1	4.7E-12	Minichromosome maintenance deficient 6
Rpl29	NM_009082.2	1.1E-11	Ribosomal protein L29
Fgfr1op2	NM_026218.1	4.9E-11	FGFR1 oncogene partner 2
Tm7sf1	XM_122498.1	2.5E-10	Transmembrane 7 superfamily member 1
Raet1c	NM_009018	1.2E-09	Retinoic acid early transcript gamma
Psmd8	NM_026545.1	2.1E-07	Proteasome (prosome macropain) 26S subunit non-ATPase 8
Cuedc1	NM_198013.1	2.2E-07	CUE domain-containing protein 1
Mgst1	NM_019946.3	3.7E-07	Microsomal glutathione *S*-transferase 1
Gdi3	NM_008112.2	6.2E-07	Guanosine diphosphate (GDP) dissociation inhibitor 3
9430077D24Rik	XM_135109	1.2E-06	RIKEN cDNA 9430077D24 gene
Rai3	NM_181444	1.3E-06	Retinoic acid induced 3
9630038C08Rik	AK036131	9.6E-05	
Cald1	AF439859.1	1.1E-04	h-caldesmon
9830123K24Rik	AK036507	1.4E-04	
Scarb2	NM_007644.2	3.0E-04	Scavenger receptor class B member 2
Cops8	NM_133805.2	3.8E-04	Constitutive photomorphogenic homolog subunit 8
5730409G07Rik	XM_126359.2	5.7E-04	RIKEN cDNA 5730409G07 gene
Atp2c1	NM_175025.2	6.8E-04	ATPase Ca^{++}-sequestering
Deadc1	NM_025748.2	8.7E-04	Deaminase domain containing 1
Ipo9	XM_129442.3	9.5E-04	Importin 9
Abhd1	NM_021304.2	1.3E-03	Abhydrolase domain containing 1
2010323F13Rik	NM_177157.2	1.9E-03	RIKEN cDNA 2010323F13 gene
2810417H13Rik	NM_026515.1	2.0E-03	RIKEN cDNA 2810417H13 gene
Thap4	NM_025920	2.3E-03	THAP domain containing 4
Pi16	NM_023734.2	2.5E-03	Peptidase inhibitor 16 precursor
Psmc4	XM_355872.1	2.5E-03	Prosome macropain 26S subunit ATPase 4
6430544H17Rik	NM_183140.1	2.6E-03	
Abhd1	NM_021304.2	2.7E-03	Abhydrolase domain containing 1
C430014G13Rik	AK049453	3.1E-03	Hypothetical protein
Tm7sf3	XM_132970.3	3.2E-03	Transmembrane 7 superfamily member 3
Acbd4	NM_025988.1	4.1E-03	Acyl-coenzyme A binding domain containing 4
Stk4	NM_021420.2	4.5E-03	Serine/threonine kinase 4
Insig2	NM_133748.1	5.5E-03	Insulin induced gene 2
Glis1	NM_147221.1	6.1E-03	GLIS family zinc finger 1
Mrpl3	AK054185	6.8E-03	Mitochondrial ribosomal protein L3
Nt5c3	NM_026004.1	6.8E-03	5-nucleotidase cytosolic III
Ugt1a9	NM_201410	7.0E-03	UDP glucuronosyltransferase 1 family, polypeptide A9
2610018I03Rik	XM_135023.2	7.1E-03	RIKEN cDNA 2610018I03 gene
B230312I18Rik	NM_172740.1	7.9E-03	RIKEN cDNA B230312I18 gene
Elmo1	NM_080288.1	8.5E-03	Engulfment and cell motility 1 ced-12 homolog
D730035F11Rik		9.1E-03	
Dgke	NM_019505	1.0E-02	Diacylglycerol kinase epsilon
E030030I06Rik	*XM_286230.2*	*9.9E-03*	*RIKEN cDNA E030030I06 gene*
Pnrc2	*NM_026383.1*	*8.2E-03*	*Proline-rich nuclear receptor coactivator 2*
Klra18	*NM_053153.1*	*8.1E-03*	*Killer cell lectin-like receptor subfamily A member 18*

Table S2. List of genes whose expression was downregulated in β3-null endothelial cells compared with wild-type (*P*<0.01).

Symbol	Accession	P-value	Definition
Rgs17	*NM_019958*	*7.6E-03*	*Regulator of G-protein signaling 17*
Agtrap	*NM_009642.3*	*7.6E-03*	*Angiotensin II type I receptor-associated protein*
Nr1d2	*NM_011584.2*	*6.7E-03*	*Nuclear receptor subfamily 1 group D member 2*
Mtap7	*NM_008635*	*6.4E-03*	*Microtubule-associated protein 7*
Klra22	*NM_053152.1*	*6.2E-03*	*Killer cell lectin-like receptor subfamily A member 22*
1810057P16Rik	*XM_126676.3*	*6.0E-03*	*RIKEN cDNA 1810057P16 gene*
E030030I06Rik	*XM_286230.2*	*5.3E-03*	*RIKEN cDNA E030030I06 gene*
1810041M07Rik	*AK007746*	*4.7E-03*	
D630046D15Rik	*AK052765*	*4.6E-03*	*Hypothetical BTB/POZ domain/Speract receptor (Scavenger receptor) containing protein*
Nt5	*AK047143*	*4.1E-03*	*5′ nucleotidase*
AI838661	*NM_133884.1*	*3.9E-03*	*Expressed sequence AI838661*
2610203C22Rik		*3.6E-03*	
Bcat1	*NM_007532.1*	*3.5E-03*	*Branched chain aminotransferase 1 cytosolic*
1810064L21Rik	*AK007954*	*2.9E-03*	
MGC67181	*NM_198619.1*	*2.8E-03*	*Unknown (protein for MGC:67181)*
3110001A05Rik	*AK013931*	*2.6E-03*	
2810408I11Rik		*2.5E-03*	
	AK021409.1	*2.4E-03*	*0 day neonate eyeball cDNA RIKEN full-length enriched library clone:E130302J09 product:hypothetical protein full insert sequence.*
LOC232532	*XM_132963.2*	*1.2E-03*	*Similar to IgE-binding protein*
Ehd3	*NM_020578.1*	*1.2E-03*	*EH-domain containing 3*
Hebp2	*NM_019487.2*	*1.1E-03*	*Heme binding protein 2*
2610305D13Rik	*NM_145078*	*1.0E-03*	*RIKEN cDNA 2610305D13 gene*
MGC67181	*NM_198619.1*	*9.3E-04*	
Raet1e	*NM_198193.1*	*9.2E-04*	*Retinoic acid early transcript 1E*
LOC381142	*XM_355058.1*	*7.3E-04*	*Similar to hypothetical protein FLJ38968*
C530044C16Rik		*2.4E-04*	
Cdkl2	*NM_177270.3*	*1.2E-04*	*Cyclin-dependent kinase-like 2 (CDC2-related kinase)*
Bcat1	*NM_007532.1*	*1.1E-04*	*Branched chain aminotransferase 1 cytosolic*
Fxr2h	*NM_011814*	*8.1E-05*	*Fragile X mental retardation gene 2 autosomal homolog*
Ybx3	*AK029441*	*8.0E-05*	*Y box protein 3*
Ppfibp1	*AK044496*	*7.9E-05*	*PTPRF interacting protein binding protein 1*
E030030I06Rik	*XM_286230.2*	*5.9E-05*	*RIKEN cDNA E030030I06 gene*
4933427D14Rik	*NM_028963.1*	*5.4E-05*	*RIKEN cDNA 4933427D14 gene*
1110005F07Rik	*NM_025383*	*1.7E-05*	*RIKEN cDNA 1110005F07 gene*
Abca5	*NM_147219.1*	*8.7E-06*	*ATP-binding cassette sub-family A (ABC1) member 5*
Hebp1	*NM_013546.1*	*8.2E-06*	*Heme binding protein 1*
Klra20	*NM_053150.1*	*4.8E-06*	*Killer cell lectin-like receptor subfamily A member 20*
Gp38	*NM_010329.1*	*1.8E-06*	*Glycoprotein 38*
LOC229810	*XM_124173.2*	*1.2E-06*	*Similar to Alpha enolase (2-phospho-D-glycerate hydro-lyase) (Non-neural enolase) (NNE) (Enolase 1)*
Itgb3	*NM_016780.1*	*6.9E-07*	*Integrin beta 3*
Raet1a	*NM_009016.1*	*4.2E-07*	*Retinoic acid early transcript 1 alpha*

Table S3. List of genes and primer sequences for real-time PCR.

Gene	Forward	Reverse
Actin	AAGGCCAACCGTGAAAAGAT	GTGGTACGACCAGAGGCATAC
β3-itgn	TCCAACATCTGTACCACACGA	GGGTGAGCCCTGAGACAA
Flk1	CAGTGGTACTGGCAGCTAGAAG	CAGTGGTACTGGCAGCTAGAAG
Rpl29	TCCGATGACATCCGTGACTA	CCATTTCTGTGCCATTTGC
Raet1γ	ATACACCAACGGGCTGGAT	CTTCGCTTCATACCAGAGAGG
Mgst1	ACTGACGAGAAGGTGGAACG	GAAGTGCATGAGGGCTGTAGA
Mcm6	ACCTGTACCACAATCTCTGCAC	CACCGCGTTTTACTTCATCA
Cuedc1	GGGACAAGTTGAAACACATGG	CTTCCTCATTTTGGTCTTCTCAG
Fgfr1op2	CCTTGAAGCACCTCAGCAC	TCTCGGTGATTTGGTCAACA
Gdl3	TGGAGGAGAAAGTGCGTCTATAA	CTGGCGGTTGTCCTGGTA
Psmd8	ATCCCTGCCGAAAGTTACAC	TAGGCCTTCTCAATGCATCC
Tm7sf1	AGTCAGAAATCCCACGAAGG	CGGGGGTTGTCAAAGAAGTA